Inorganic Chemistry

Article

pubs.acs.org/IC

Low-Spin Hexacoordinate Mn(III): Synthesis and Spectroscopic Investigation of Homoleptic Tris(pyrazolyl)borate and Tris(carbene)borate Complexes

Adam P. Forshaw,[†] Jeremy M. Smith,*[,†] Andrew Ozarowski,[‡] J. Krzystek,[‡] Dmitry Smirnov,[‡] S. A. Zvyagin,[§] T. David Harris,[∥] Hemamala I. Karunadasa,[⊥] Joseph M. Zadrozny,[#] Alexander Schnegg,[▽] Karsten Holldack,[○] Timothy A. Jackson,[◇] Ahmad Alamiri,[¶] Diane M. Barnes,[¶] and Joshua Telser*[,¶]

[†]Department of Chemistry and Biochemistry, New Mexico State University, Las Cruces, New Mexico 88003, United States

[‡]National High Magnetic Field Laboratory (NHMFL), Florida State University, Tallahassee, Florida 32310, United States

[§]Dresden High Magnetic Field Laboratory (HLD), Helmholtz-Zentrum Dresden-Rossendorf, D-01314 Dresden, Germany

[∥]Department of Chemistry, Northwestern University, Evanston, Illinois 60208, United States

[⊥]Department of Chemistry, Stanford University, Stanford, California 94305, United States

[#]Department of Chemistry, University of California, Berkeley, California 94720, United States

[▽]Helmholtz-Zentrum für Materialien und Energie, Institut für Silizium-Photovoltaik, D-12489 Berlin, Germany

[○]Helmholtz-Zentrum für Materialien und Energie, Institut für Methoden und Instrumente der Forschung mit Synchrotronstrahlung, D-12489 Berlin, Germany

[◇]Department of Chemistry, University of Kansas, Lawrence, Kansas 66045, United States

[¶]Department of Biological, Chemical and Physical Sciences, Roosevelt University, Chicago, Illinois 60605, United States

Supporting Information

ABSTRACT: Three complexes of Mn(III) with "scorpionate" type ligands have been investigated by a variety of physical techniques. The complexes are $[Tp_2Mn]SbF_6$ (**1**), $[Tp_2{*}Mn]SbF_6$ (**2**), and $[\{PhB(MeIm)_3\}_2Mn](CF_3SO_3)$ (**3a**), where Tp^- = hydrotris(pyrazolyl)borate anion, Tp^{*-} = hydrotris(3,5-dimethylpyrazolyl)borate anion, and $PhB(MeIm)_3^-$ = phenyltris(3-methylimidazol-2-yl)borate anion. The crystal structure of **3a** is reported; the structures of **1** and **2** have been previously reported, but were reconfirmed in this work. The synthesis and characterization of $[\{PhB(MeIm)_3\}_2Mn]Cl$ (**3b**) are also described. These complexes are of interest in that, in contrast to many hexacoordinate (pseudo-octahedral) complexes of Mn(III), they exhibit a low-spin (triplet) ground state, rather than the high-spin (quintet) ground state. Solid-state electronic absorption spectroscopy, SQUID magnetometry, and high-frequency and -field electron paramagnetic resonance (HFEPR) spectroscopy were applied. HFEPR, in particular, was useful in characterizing the $S = 1$ spin Hamiltonian parameters for complex **1**, $D = +19.97(1)$, $E = 0.42(2)$ cm^{-1}, and for **2**, $D = +15.89(2)$, $E = 0.04(1)$ cm^{-1}. In addition, frequency domain Fourier-transform THz-EPR spectroscopy, using coherent synchrotron radiation, was applied to **1** only and gave results in good agreement with HFEPR. Variable-temperature dc magnetic susceptibility measurements of **1** and **2** were also in good agreement with the HFEPR results. This magnitude of zero-field splitting (zfs) is over 4 times larger than that in comparable hexacoordinate Mn(III) systems with $S = 2$ ground states. Complexes **3a** and **3b** (i.e., regardless of counteranion) have a yet much larger magnitude zfs, which may be the result of unquenched orbital angular momentum so that the spin Hamiltonian model is not appropriate. The triplet ground state is rationalized in each complex by ligand-field theory (LFT) and by quantum chemistry theory, both density functional theory and unrestricted Hartree−Fock methods. This analysis also shows that spin-crossover behavior is not thermally accessible for these complexes as solids. The donor properties of the three different scorpionate ligands were further characterized using the LFT model that suggests that the tris(carbene)borate is a strong σ-donor with little or no π-bonding.

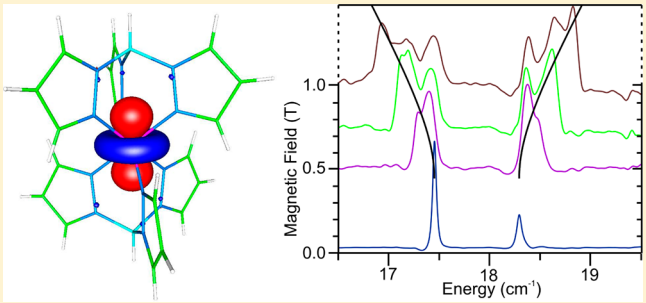

INTRODUCTION

The tris(pyrazolyl)borate anion (Tp^-),[1] the common ancestor of all scorpionate ligands, has proven to be an extremely versatile supporting ligand. Compounds containing Tp^- (or

Received: July 25, 2012
Published: December 24, 2012

   dx.doi.org/10.1021/ic301630d | Inorg. Chem. 2013, 52, 144−159

one of its multitude of substituted variants) have been made for all transition metals, most lanthanides, and many main group elements.[2−4] New families of scorpionate ligands have subsequently evolved; in these next-generation ligands, the original pyrazolyl donors have been replaced by groups based on carbon, sulfur, or phosphorus donors.[5−7] Our contribution to this field has been in the development of tris(carbene)borate ligands, a family of scorpionates that provide a facial N-heterocyclic carbene donor set.[8−10]

Without the additional steric bulk provided by suitable pyrazolyl substituents, tris(pyrazolyl)borate ligands typically form homoleptic complexes with first row transition metals. In these complexes, two scorpionate ligands are bound to the metal in a trigonally distorted octahedral geometry. Modifying the ligand substituents while still maintaining the geometry is straightforward, making these complexes suitable for detailed spectroscopic and electronic structure studies. For example, a detailed magnetic resonance spectroscopy and electronic structure study of a series of structurally similar $Tp_2Co(II)$ ($S = 3/2$, $3d^7$) complexes allowed for facile interpretation of EPR data when O_h Co(II) is otherwise notoriously difficult to understand.[11,12]

Another transition-metal ion that commonly forms octahedral HS complexes is Mn(III) ($3d^4$, $S = 2$). Interestingly, the homoleptic hydrotris(pyrazolyl)borate complexes $[Tp_2Mn]SbF_6$ (**1**) and $[Tp_2*Mn]SbF_6$ (**2**) ($Tp*^-$ = hydrotris(3,5-dimethylpyrazolyl)borate) were found by Schultz and coworkers to have the low-spin (LS, in octahedral symmetry) configuration ($S = 1$) as the ground state.[13] As part of our long-term project to investigate mononuclear transition-metal complexes with $S > 1/2$, in particular, those with large zero-field splitting (zfs), employing high-frequency and -field electron paramagnetic resonance (HFEPR), we have turned our attention to these two Mn(III) complexes. We note that it has been pointed out that complexes of Mn(III) are "widely recognized as the *deliciae* of HFEPR spectroscopists".[14] However, this statement was in reference to "traditional" HS Mn(III); whether this was applicable also to LS Mn(III) had yet to be determined.

To gain additional insight, we have also investigated the structurally related, but more strongly donating, N-heterocyclic carbene (NHC) analogue of these complexes, the bis(phenyltris(3-methylimidazol-2-yl)borate)manganese(III) cation, both as its triflate $[\{PhB(MeIm)_3\}_2Mn](CF_3SO_3)$ (**3a**) and chloride $[\{PhB(MeIm)_3\}_2Mn]Cl$ (**3b**) salts, which are reported for the first time here. The triflate complex (**3a**) was characterized by single-crystal X-ray diffraction as well as the same physical methods used for the tris(pyrazolyl)borate complexes.

We show here that HFEPR can be readily applied to the two tris(pyrazolyl)borate complexes and that this technique, in combination with solid-state magnetometry, clearly indicates the orbitally nondegenerate spin triplet ground state for both. The tris(carbene)borate complex is a more complicated case and may have a ground state that is orbitally degenerate. The electronic structure of the three complexes is probed by ligand-field theory (LFT) and by quantum chemistry theory (QCT), including both density functional theory (DFT) and unrestricted Hartee−Fock (UHF) methods.

EXPERIMENTAL SECTION

General Procedures. All manipulations were performed under a nitrogen atmosphere by standard Schlenk techniques or in an M. Braun Labmaster glovebox maintained at or below 1 ppm of O_2 and H_2O. Glassware was dried at 150 °C overnight. ^1H NMR data were recorded on a Varian Unity 400 spectrometer (400 MHz) at 22 °C. Acetonitrile (MeCN), diethyl ether (Et_2O), tetrahydrofuran (THF), and toluene were purified by the Glass Contour solvent purification system. Before use, aliquots of Et_2O, THF, and toluene were tested with a drop of sodium benzophenone ketyl in THF solution. Acetonitrile-d_3 was stored over molecular sieves. Celite was dried overnight at 200 °C under vacuum. The tris(carbene)borate ligand precursor $PhB(MeImH)_3(CF_3SO_3)_2$ was prepared according to a published procedure.[15] Lithium diisopropylamide (LDA) was prepared by addition of ^{n}BuLi to a solution of diisopropylamine in pentane at −78 °C and stored at −35 °C. All other chemicals were obtained commercially and used as received. All resonances in the ^1H NMR spectra are referenced to residual CD_2HCN at δ 1.94 ppm. Electrospray mass spectral data were collected using a Waters-Micromass ZQ2000 mass spectrometer using MeCN as the solvent. Elemental analyses were determined by Desert Analytics, Tucson, AZ, and the Microanalytical Facility at the University of California, Berkeley.

Synthesis. *Synthesis of Complexes 1 and 2.* These complexes were initially obtained as gifts from Prof. F. A. Schultz (IUPUI). The complexes were also synthesized from KTp and KTp*, respectively, and $Mn(OAc)_2{\cdot}4H_2O$ to yield Tp_2Mn and $Tp*_2Mn$, respectively,[16] which were oxidized with $NOSbF_6$ according to a literature procedure.[13] Elemental analysis $[Tp_2Mn]SbF_6$ (**1**): Anal. Calcd for $C_{18}H_{20}B_2F_6MnN_{12}MnSb$: C, 30.16; H, 2.81; N, 23.45. Found: C, 29.91; H, 2.97; N, 23.19; $[Tp*_2Mn]SbF_6$ (**2**): Anal. Calcd for $C_{30}H_{44}B_2F_6MnN_{12}MnSb$: C, 40.71; H, 5.01; N, 18.99. Found (for two independently prepared batches, each used for magnetometric measurements; second batch in parentheses): C, 40.53 (40.92); H, 5.18 (5.00); N, 18.92 (19.12).

Both sources of **1** and **2** were used for HFEPR and UV−vis spectroscopy, giving identical results. Crystalline, analytically pure, independently prepared complexes were used for magnetometry.

Synthesis of [{PhB(MeIm)$_3$}$_2$Mn]. From MnBr$_2$. A solution of LDA (260 mg, 2.45 mmol) in THF (7 mL) was added dropwise to a stirring solution of $PhB(MeImH)_3(CF_3SO_3)_2$ (500 mg, 791 μmol) in THF (5 mL). The reaction mixture was stirred for 7 h, producing an off-white precipitate. Solid $MnBr_2$ (85 mg, 396 μmol) was added, and the mixture was stirred overnight. The resulting dark orange solution was dried under vacuum to yield a dark orange solid. The solid was extracted with toluene, filtered through Celite, and dried to yield orange-red $[\{PhB(MeIm)_3\}_2Mn]$ (98 mg, 17%). Analytically pure product was crystallized by vapor diffusion of pentane into a saturated THF solution.

From [{PhB(MeIm)$_3$}$_2$Mn](CF$_3$SO$_3$)$_2$. Solid $[\{PhB(MeIm)_3\}_2Mn](CF_3SO_3)_2$ (250 mg, 0.21 mmol), prepared as described previously,[15] was added to a mixture of excess KC_8 (70 mg) in THF (10 mL). The reaction was stirred for 2 h, filtered through Celite, and dried to yield dark orange $[\{PhB(MeIm)_3\}_2Mn]$ (128 mg, 70%). UV−vis (MeCN): λ_{max} = 408 nm (ε = 9400 M·cm^{-1}), 318 nm (ε = 7800 M·cm^{-1}), 282 nm (ε = 7700 mol·cm^{-1}). ESI-MS m/Z^+: = 717. Anal. Calcd for $C_{26}H_{40}B_2N_6Mn{\cdot}C_5H_{12}$: C, 62.37; H, 6.64; N, 21.29. Found C, 62.91; H, 6.21; N, 22.74.

*Synthesis of [{PhB(MeIm)$_3$}$_2$Mn]Cl (**3b**).* A solution of LDA (260 mg, 2.45 mmol) in THF (7 mL) was added dropwise to a stirring solution of $PhB(MeImH)_3(CF_3SO_3)_2$ (500 mg, 791 μmol) in THF (5 mL). The reaction mixture was stirred for 7 h, producing an off-white precipitate. Solid $MnBr_2$ (85 mg, 396 μmol) was added, and the mixture was stirred overnight. The resulting dark orange solution was dried under vacuum to yield a dark orange solid. Dichloromethane (15 mL) was added, and the solution was left to stir overnight, producing a yellow solution. The solution was filtered through a Celite pad and dried to yield pale yellow $[\{PhB(MeIm)_3\}_2Mn]Cl$ (297 mg, 100%). ^1H NMR (400 MHz, CD_3CN, 22 °C) δ 15.1 (m, 2H, *o*/*m*-H); 10.6 (m, 2H, *o*/*m*-H); 9.9 (t, J_{HH} = 2 Hz, 1H, *p*-H); 8.2 (s, 3H Im-H); 6.6 (s, 9H, M-H); −7.3 (s, 3H, Im-H). μ_{eff} (Evans'): 2.3(3) BM. UV−vis (MeCN) λ_{max}: 385 nm (ε = 3000 M·cm^{-1}), 250 nm (sh). Anal. Calcd

dx.doi.org/10.1021/ic301630d | Inorg. Chem. 2013, 52, 144−159

for $C_{26}H_{40}B_2N_6MnCl\cdot1.5CH_2Cl_2$: C, 51.17; H, 4.92; N, 19.10. Found: C, 51.19; H, 4.67; N, 18.39.

*Synthesis of [{PhB(MeIm)$_3$}$_2$Mn]CF$_3$SO$_3$ (**3a**).* A solution of LDA (260 mg, 2.45 mmol) in THF (7 mL) was added dropwise to a stirring solution of $PhB(MeImH)_3(CF_3SO_3)_2$ (500 mg, 791 μmol) in THF (5 mL). The reaction mixture was stirred for 7 h, producing an off-white precipitate. Solid $MnBr_2$ (85 mg, 396 μmol) was added, and the mixture was stirred overnight. The resulting dark orange solution was dried under vacuum to yield a dark orange solid. Dichloromethane (15 mL) was added, and the solution was left to stir overnight, producing a yellow solution. The solution was filtered through a Celite pad and dried to yield pale yellow [{PhB(MeIm)$_3$}$_2$Mn]Cl (**3b**). The solid was redissolved in MeCN (5 mL), and KCF_3SO_3 (461 mg, 2.45 mmol) was added. After stirring for 1 h, the solution was filtered and crystallized by slow diffusion of Et_2O into the MeCN solution. The product was obtained as a yellow powder after drying under vacuum (80%).

^{1}H NMR (400 MHz, CD_3CN): 15.1 (m, 2H, *o*/*m*-H); 10.6 (m, 2H, *o*/*m*-H); 9.9 (t, J_{HH} = 2 Hz, 1H, *p*-H); 8.2 (s, 3H Im-H); 6.6 (s, 9H, M-H); −7.3 (s, 3H, Im-H). μ_{eff} (Evans'): 2.3(3) BM. UV−vis (MeCN) λ_{max}: 385 nm (ε = 3115 M·cm^{-1}), 250 nm (sh).

X-ray Crystallography. Large orange crystals of **1** were formed by slow evaporation of an acetonitrile solution in air. X-ray diffraction (Bruker Platform Apex II diffractometer with Mo source) showed unit cell dimensions that were essentially identical with those reported.[17] Small yellow crystals of **2** were grown by slow evaporation of an acetonitrile/toluene (1:1 v/v) solution in air. X-ray diffraction as above showed unit cell dimensions that were essentially identical with those reported.[18]

Crystals of **3a** suitable for X-ray diffraction were grown by diffusion of THF into a solution of the complex in MeCN at −25 °C. A crystal was coated with Paratone-N oil, mounted on a Kaptan loop, and cooled under a stream of N_2. Data were collected with a Bruker MICROSTAR X-ray source, APEX-II detector and Cu anode (λ = 1.5406 Å). Raw data were integrated and corrected for Lorentz and polarization effects using Bruker APEX2, v.2009.1.[19] Absorption corrections were applied using SADABS.[20] The space group assignment was based upon systematic absences, *E*-statistics, agreement factors for equivalent reflections, and successful refinement of the structure. The structure was solved by direct methods and expanded through successive difference Fourier maps. It was refined against all data using the SHELXTL 5.0 software package.[21] Hydrogen atoms were inserted at idealized positions and refined using a riding model with an isotropic thermal parameter 1.2 times that of the attached carbon atom (or 1.5 times for terminal methyl groups). Thermal parameters for all non-hydrogen atoms were refined anisotropically, except for the disordered atoms in the solvent and counterions. The program SQUEEZE[22] was employed to account for the disordered solvent and counterions in **3a**, which, based on the electron count, were identified as two triflate anions and two THF molecules per unit cell.

Electronic Absorption Spectroscopy. Spectra were recorded on a Jasco V-570 spectrophotometer in Suprasil cuvettes. Acetonitrile-d_3 was used to record solution NIR spectra to reduce interference from C−H overtones. A diffuse reflectance accessory was used to record spectra of solids mixed with MgO.

Magnetic Susceptibility. Magnetic data were collected using a Quantum Design MPMS-XL magnetometer. Measurements for compounds **1**, **2**, and **3b** were obtained on finely ground microcrystalline powders restrained under eicosane within polycarbonate capsules. Direct current (dc) magnetic susceptibility data were collected in the temperature range of 2−300 K under an applied field of 1000 Oe. All data were corrected for diamagnetic contributions from the sample holder and restraint as well as for core diamagnetism (estimated using Pascal's constants).[23,24] The data were fitted using a spin Hamiltonian for S = 1 (see eq 1 below), but with only axial zero-field splitting terms (i.e., E = 0) and isotropic g. This procedure has been used by some of us previously, and the software is available from J. Telser.

HFEPR Data Acquisition. HFEPR spectra were recorded using facilities at the National High Magnetic Field Laboratory (NHMFL, Tallahassee, FL), the Electron Magnetic Resonance (EMR) Facility[25] and the Millimeter and Submillimeter Wave Facility,[26] and at the Dresden High Magnetic Field Laboratory (HLD, Dresden, Germany). Both laboratories employ tunable millimeter and submillimeter wave radiation sources, including backward wave oscillators (BWOs) and a variety of solid-state generators, in conjunction with 15/17 T (NHMFL) and 16 T (HLD) superconducting or 25 T resistive ("Keck", NHMFL) magnets. Detection was provided in each case with an InSb hot-electron bolometer (QMC Ltd., Cardiff, U.K.). Modulation for detection purposes was provided alternatively by chopping the sub-THz wave beam ("optical modulation") or by modulating the magnetic field. The relative merits of both types of modulation were discussed in a previous paper by some of us.[27] A standard lock-in amplifier (Stanford Research Systems SR830) converted the modulated signal to dc voltage.

Ground powders (typically, 30−50 mg) of **1** or **2** were loaded into Teflon sample holders in air and gave good quality HFEPR spectra (see below). Samples of **3b** were prepared in these holders in an Ar-filled glovebag but became partially oxidized and gave no HFEPR spectra at frequencies up to 400 GHz. A sample of this complex was also prepared under Ar in a sealed Suprasil tube and gave no evidence of oxidation (rapid color change from yellow to purple); however, this sample also gave no HFEPR spectra, although the maximum usable frequency was only 400 GHz, due to excessive absorption by the tube at higher values.

HFEPR Data Analysis. The single-frequency HFEPR spectra were fitted using a spin Hamiltonian for S = 1 systems composed of Zeeman and zero-field splitting (zfs) terms:[28]

$$\mathcal{H} = \beta_e B\cdot g\cdot \hat{S} + D(\hat{S}_z^{\,2} - S(S+1)/3) + E(\hat{S}_x^{\,2} - \hat{S}_y^{\,2}) \qquad (1)$$

Individual powder-pattern spectra at multiple frequencies were simulated using this spin Hamiltonian, which allows direct extraction of the zfs parameters D and E, along with the g values. To provide frequency-independent parameters, and refine them, computer fits were made to two-dimensional field versus frequency data sets. Further details of the tunable-frequency HFEPR methodology are given elsewhere.[27]

FD-FT THz-EPR Data Acquisition. Frequency domain Fourier transform (FD-FT) THz-EPR spectroscopy was performed in a special electron optical mode (the low α mode) of the BESSY II storage ring,[29] which is optimized for the generation of stable ultrashort (∼2 ps) electron pulses emitting broad-band high-power (>10 mW) radiation in the frequency range of ν = 150 GHz−1.2 THz (5−40 cm^{-1}).[30] The coherent synchrotron radiation (CSR) is coupled out of the accelerator by a low-loss quasi-optical THz transmission line through a *z*-cut quartz window serving as a radiation outlet on top of the storage ring. The THz beam propagating in (vacuum) free space is then focused on the external radiation port of a high-resolution FTIR-spectrometer (Bruker IFS125 HR, max. res. 0.0063 cm^{-1}) by off-axis parabolic mirrors. Detection is obtained by a liquid-helium-cooled Si bolometer. Sample temperature and magnetic field were controlled using a liquid-helium-cooled cryostat (Oxford Optistat, T = 1.5−300 K) or, alternatively, an SC magnet with a variable-temperature insert (Oxford Spectromag 4000; B_0 = ±10 T, T = 1.5−300 K), both equipped with THz transparent windows, into the beam path. To correct for changes in the frequency-dependent emission spectrum over time and to discriminate electric dipole transitions in the sample material from spin-induced magnetic dipole transitions, FT reference spectra, $I_0(\nu)$, taken at thermal energies well above the energy of the ground-state spin transitions (e.g., 40 K) were divided by $I(\nu)$, the FT spectra taken at very low temperature (e.g., 2 K). Thereby, ground-state spin transitions may be recorded as spectral absorptance (equivalent to [1 − transmittance]) changes originating from temperature-dependent population changes of the spin levels. Because of limitations on beamtime availability and the extreme air sensitivity of **3a** and **3b**, only complex **1** was investigated by this technique. The sample was prepared by grinding with powdered PTFE (80 mg

dx.doi.org/10.1021/ic301630d | *Inorg. Chem.* 2013, 52, 144−159

sample, 150 mg PTFE), and the mixture was then pressed into a pellet (10 mm diameter, 2 t of pressure).

LFT Analysis. Analysis of the electronic structure of Mn(III) in the studied complexes was performed with the use of two approaches: crystal-field parametrization, as described by Ballhausen,[31] and the angular overlap model (AOM), originally due to Schäffer.[32,33] Two computer programs were employed, Ligfield, written by J. Bendix (Ørsted Institute, Copenhagen, Denmark),[34] and a locally written program, DDN, available from J. Telser. Both programs use the complete d^4 weak-field basis set, including interelectronic repulsion (Racah parameters: B and C) and spin−orbit coupling (SOC) and either crystal-field (for DDN, the parameters: Dq, Ds, Dt,[31] Dr} or AOM ligand-field bonding parameters (ε_σ, ε_π).[33] The two programs gave identical results when directly compared. The Ligfield program allows identification of the orbital occupancy and spin progeny of a given energy level (eigenstate).

Various sources are available for both Racah parameters and SOC constants for d block free-ions.[33,35] We have now determined that there is only one rigorously analyzed and documented source for each of these parameters: Racah parameters are given by Brorson and Schäffer[36] and SOC constants are given by Bendix, Brorson, and Schäffer.[34,37] In this work, we have, therefore, used for free-ion Mn(III), B = 950 cm^{-1}, C = 4112 cm^{-1} (C = 4.33B), and for free-ion Cr(III) (for which we did comparative calculations), B = 933 cm^{-1}, C = 3710 cm^{-1} (C = 3.97B).

In contrast to other systems studied by us,[10] the electronic absorption spectra for the complexes of interest do not allow definitive identification of d−d transitions (see below). Therefore, no fitting of electronic transitions using LFT parameters was performed. Instead, as described below, parameters adapted from related systems were used,[38] which gave results consistent with experiment, and the SOC was adjusted to match the observed zfs data as best as possible.

QCT Analysis. All quantum chemical computations employed the software package ORCA (version 2.9), written by Neese and co-workers.[39] Two theoretical methods were employed: density functional theory (DFT) and unrestricted Hartree−Fock (UHF) theory. Geometry optimizations using DFT were performed at the spin-unrestricted level using the BP functional,[40−42] with TZVP (Mn and coordinating N or C atoms) and SVP (noncoordinating N and C atoms and B and H atoms) basis sets. The DFT calculations of electronic structure utilized the B3LYP/G functional (i.e., the B3LYP formulation as defined in the Gaussian program suite)[41−44] and were performed at the spin-unrestricted level. Both DFT and UHF calculations utilized the TZVPP basis set[45,46] for Mn and coordinating N or C atoms and the SVP basis set for all other atoms. The RIJCOSX approximation[47] was utilized along with appropriate auxiliary basis sets from the TurboMole library (ftp.chemie.uni-karlsruhe.de/pub/jbasen), as defined elsewhere.[43,48,49] Ground-state spin Hamiltonian parameters (i.e., g values and the **D** tensor) were calculated using structures obtained from both X-ray crystallography and DFT geometry optimizations. These calculations employed the so-called coupled-perturbed method for calculating the **D** tensor, which is described in detail elsewhere.[50] Quasi-restricted orbitals[51] were visualized using the program gOpenMol.[52,53] A representative ORCA input/output file (for $[Tp_2Mn]^+$) is given in the Supporting Information (Table S5).

RESULTS AND DISCUSSION

Synthesis. Addition of one-half equivalent of $MnBr_2$ to in situ generated "PhB(MeIm)$_3$Li"[15] leads to the isolation of a dark orange solid, which has been characterized as $[\{PhB(MeIm)_3\}_2Mn]$ by ESI-MS and elemental analysis. The complex is more conveniently prepared by a two-electron reduction of the previously reported[15] Mn(IV) complex $[\{PhB(MeIm)_3\}_2Mn](CF_3SO_3)_2$. Thus far, $[\{PhB(MeIm)_3\}_2Mn]$ has eluded crystallization, precluding characterization by X-ray diffraction methods. Analysis by ^1H NMR has also proven impossible because $[\{PhB(MeIm)_3\}_2Mn]$ is NMR silent. Additionally, the very low solubility of this complex has prevented determination of the effective magnetic moment by the Evans method. This complex reacts with strong oxidants (e.g., O_2, NO^+, and Ag^+) to reform the Mn(IV) complex.[15] By contrast, $[\{PhB(MeIm)_3\}_2Mn]$ reacts with CH_2Cl_2 to quantitatively yield the pale yellow Mn(III) complex $[\{PhB(MeIm)_3\}_2Mn]Cl$ (**3b**). This reaction occurs even in the dark, indicating that it is a ground-state reaction of the Mn(II) complex, and no photoinitiated radicals are involved. Other chlorinated solvents, namely, CCl_4, $CHCl_3$, and C_6H_5Cl, oxidize $[\{PhB(MeIm)_3\}_2Mn]$ to yield **3b**, with the qualitatively determined relative rate of oxidation $CCl_4 > CHCl_3 > C_6H_5Cl$. This behavior of $[\{PhB(MeIm)_3\}_2Mn]$ contrasts with the tris(pyrazolyl)borate congeners, Tp_2Mn and Tp^*_2Mn, which are air-stable and crystallized from CH_2Cl_2.[16] This comparison suggests, unsurprisingly, that the strong σ-donating carbene units in $[\{PhB(MeIm)_3\}_2Mn]^+$ shift the Mn(II)/Mn(III) couple to a more negative potential relative to the tris(pyrazolyl)borate analogue.[54]

Compound **3b** is also extremely air-sensitive, rapidly developing a purple color (indicative of Mn(IV)) when exposed to air. Reaction of this chloride salt with KCF_3SO_3 allows for anion metathesis, providing $[\{PhB(MeIm)_3\}_2Mn]CF_3SO_3$ (**3a**) in high yield.

In contrast to NMR-silent $[\{PhB(MeIm)_3\}_2Mn]$, **3b** displays a paramagnetically shifted ^1H NMR spectrum in which all of the resonances can be assigned. In CD_3CN solution, two broad resonances at δ −7.3 and δ 8.3 ppm are assigned to the imidazol-2-ylidene protons. A broad resonance at δ 6.8 ppm is assigned to the methyl protons. Two multiplets at δ 15.2 ppm and δ 10.7 ppm are assigned to the *meta* and *ortho* protons of the phenyl group, respectively, while a triplet at δ 10.0 ppm is assigned to the *para* proton.

Structures. The crystal structures of **1** and **2** have been previously reported by Schultz and co-workers.[13] We will briefly discuss salient features of these structures as they relate to the LFT analysis given below. The relevant metrical parameters are given in Tables S1−S3 (Supporting Information). The structure of **3a** has not been previously reported and will be discussed in more detail.

The crystal structure of **1** is densely packed (cell volume = 624 Å^3; Z = 1), and the Mn(III) ion of the molecular cation and nearest Sb(V) ion of the counteranion are separated by only 6.13 Å. The variations in Mn−N distances and N−Mn−N angles are slight (see Table S1, Supporting Information), and the angles are close to the value of 90° for ideal N6 octahedral coordination. The $[Tp_2Mn]^+$ complex has an inversion center and almost perfect 3-fold symmetry with the C_3 rotation axis defined by the B1−Mn−B1A vector, which leads to the projection of the N−B(1 or 1A)−N(adjacent pyrazole) angles normal to the B1−Mn−B1A axis all being almost exactly 60° (these correspond to ϕ for the AOM; see below and Table S2, Supporting Information).

The molecular structure of **2** is very similar, although the crystal packing is less dense (cell volume = 1828 Å^3; Z = 2, so 914 Å^3/molecular unit), and the Mn(III) and nearest Sb(V) ions are separated by 7.80 Å. The $[Tp^*_2Mn]^+$ complex has an inversion center and almost perfect 3-fold symmetry with nearly ideal 60° dihedral angles, as described above for **1**. Both complexes **1** and **2** are essentially textbook examples of immediate octahedral symmetry and overall trigonal symmetry due to the coordination of two tridentate scorpionate ligands.

Compound **3a** crystallizes in the triclinic space group $P\bar{1}$. Relevant crystallographic parameters for this complex are given

dx.doi.org/10.1021/ic301630d | Inorg. Chem. 2013, 52, 144−159

in Table 1. The asymmetric unit consists of two half-molecules with the manganese ions lying on crystallographic inversion

Table 1. Crystallographic Data for $[\{PhB(MeIm)_3\}_2Mn]CF_3SO_3$ (Complex 3a)

empirical formula	$C_{37}H_{42}B_2F_3MnN_{12}O_3S$
formula wt	868.44
temp	100(2) K
cryst syst, space group	triclinic, $P\bar{1}$
unit cell dimensions	a = 9.8644(5) Å
	b = 11.6252(6) Å
	c = 19.6618(8) Å
	α = 89.670(4)°
	β = 86.084(4)°
	γ = 88.167(4)°
volume	2248.30(19) Å^3
Z, calcd density	2, 1.384 Mg m^{-3}
abs coeff	3.403 mm^{-1}
reflns collected/unique	9014/5917 [R(int) = 0.0226]
GOF on F^2	1.190
final R indices [$I > 2\sigma(I)$]	R_1 = 0.0848,[a] wR_2 = 0.2473[b]
R indices (all data)	R_1 = 0.0968, wR_2 = 0.2600
largest diff. peak and hole	1.394 and −0.393 e·Å^{-3}

[a] $R_1 = \sum||F_o| - |F_c||/\sum|F_o|$(based on reflections with $I > 2\sigma(I)$). [b] $wR_2 = [\sum w(|F_o| - |F_c|)^2/\sum w|F_o|2]^{1/2}$; $w = 1/[\sigma^2(F_o^2) + (0.0320P)^2 + 1.39P]$; $P = [\max(F_o^2,0) + 2F_c^2]/3$ (all data).

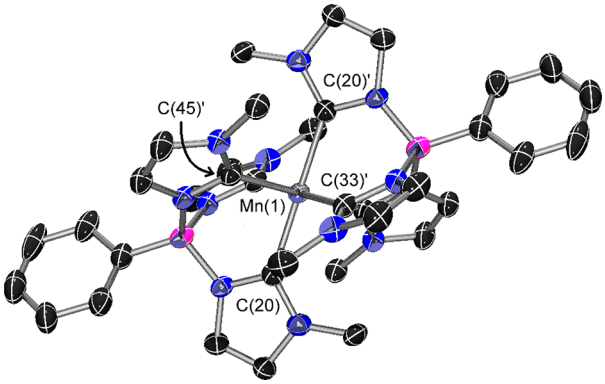

Figure 1. Molecular structure of the cation of $[\{PhB(MeIm)_3\}_2Mn]CF_3SO_3$ (**3a**) showing atomic labeling scheme. Thermal ellipsoids are shown at 50% probability; hydrogen atoms and triflate anions are omitted for clarity. Selected bond lengths (Å) and angles (deg): Mn(1)−C(45) 2.014(5); Mn(1)−C(33) 2.028(5); Mn(1)−C(20) 2.037(5); C(45)′−Mn(1)−C(33) 86.96(18); C(45)′−Mn(1)−C(20) 87.29(18); C(33)−Mn(1)−C(20) 85.8(2). Symmetry operation to generate equivalent atoms: $-x, -y, -z$.

centers (Figure 1). Both molecules have similar metrical parameters with Mn−C bonds lengths in the ranges of 2.014(5)−2.039(5) and 2.019(5)−2.054(5) Å. The small variation in these bond lengths is consistent with the low-spin electronic configuration of the d^4 Mn(III) ion (see below). Table S1 (Supporting Information) provides relevant bond lengths for Mn(II), Mn(III), and Mn(IV) scorpionates. Interestingly, and in contrast to the structurally related tris(pyrazolyl)borate complexes $[Tp^{III}{}_2{}^*Mn]^{+1}$[3] and $[Tp^{IV}{}_2{}^*Mn]^{2+}$,[55] where there is a slight decrease (~0.03 Å) in the Mn−N bond lengths on oxidation,[56] the Mn−C bond lengths in **3a** show no significant difference from those observed in the Mn(IV) congener.[15] The reasons for this difference are unclear but may be related simply to steric interactions among the methyl groups of the tris(carbene)-borate ligands that prevent the formation of shorter Mn−C bonds in the Mn(IV) complex. There might also be changes in electronic structure between the two that are not understood. As an indication of the possibly unusual nature of the tris(carbene)borate Mn(IV) complex, we note the extreme ease of oxidation of Mn(III) to Mn(IV) compared to the tris(pyrazolyl)borates.[15] The detailed electronic structure of the Mn(IV) congener will be the subject of a future study.

Not surprisingly, given the topological similarities of the tris(carbene)borate and tris(pyrazolyl)borate ligands, the structure of **3a** shares many similarities with those of **2**. For example, due to the *cis* C−Mn−C bond angles in the tris(carbene)borate being slightly smaller than 90°, there is a small trigonal distortion, leading to effective D_{3d} symmetry at the metal center. Furthermore, the Mn−C−N−C torsions and M−C−N−B torsions in **3a** are close to 180° and 0°, while the average distance between methyl groups of the tris(carbene)-borate ligands is 3.7 Å, the same as observed in **2**. The E−Mn−E (E = N, C) bond angles are essentially unchanged upon oxidation of all three complexes studied here (see Table S1, Supporting Information).

Electronic Absorption Spectroscopy. The UV−vis solution spectra of **1** and **2** have been previously reported.[13,57,58] Both complexes exhibited strong bands ($\varepsilon \approx 10^4$ M^{-1} cm^{-1}) in the near-UV region (~270 and ~350 nm). By analogy with the many other $(Tp^{R,R'})_2M$ complexes that have been reported,[2,59] these bands are assigned to metal-to-ligand charge transfer (MLCT) transitions.[60] There was also a shoulder at 385−390 nm in $[Tp_2Mn]^+$ and at 410−415 nm in $[Tp^*{}_2Mn]^+$, which was assigned to a d−d transition,[57] although Schultz and co-workers were not absolute in this assignment.[13]

The UV−vis spectra of $[Tp_2Mn]^+$ and $[Tp^*{}_2Mn]^+$ were recorded here in both 1,2-dichloroethane and MeCN solutions at room temperature and are essentially identical to those reported previously.[13] The UV−vis spectrum of $[\{PhB(MeIm)_3\}_2Mn]^+$ is very similar to those of the two tris(pyrazolyl)borate complexes, albeit with a roughly 3-fold lower molar absorptivity, which was confirmed by a Beer−Lambert law analysis. The MeCN solution spectra of the three complexes are presented in Figure S2 (Supporting Information). In addition, NIR spectra (900−2000 nm) were recorded in CD_3CN solution, but showed no absorption from any of the three Mn(III) complexes.

Our solution-phase electronic absorption spectra of the two tris(pyrazolyl)borate complexes confirm previous work[13,57] and show the correspondence with the tris(carbene)borate complex. However, our focus here is on the solid-state properties of these complexes. Therefore, diffuse reflectance spectra at room temperature in the vis and NIR regions of solid **1**, **2**, and **3b** were recorded here, using MgO as a diluent, and are shown in Figure 2. Complex **1** exhibits the main near-UV band at 390−395 nm and a shoulder at 460−465 nm. In contrast, the main band and shoulder for **2** appear at ~400 and 475 nm, respectively. The reflectance spectrum of **3b** displays two broad bands, each of which appear to have two respective components: one at 400 and 440 nm, and the other at 515 and 565 nm.

The definitive assignment of both the solid-state and the solution-phase electronic absorption spectra of the complexes

dx.doi.org/10.1021/ic301630d | Inorg. Chem. 2013, 52, 144−159

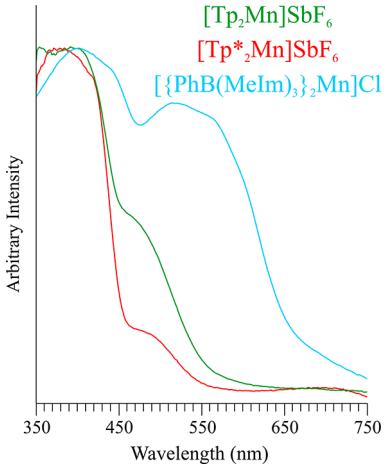

Figure 2. Electronic reflectance spectra of $[Tp_2Mn]SbF_6$ (**1**, green trace), $[Tp^*_2Mn]SbF_6$ (**2**, red trace), and $[\{PhB(MeIm)_3\}_2Mn]Cl$ (**3b**, sky blue trace), at room temperature, recorded with MgO diluent. The ordinate is arbitrary, and the spectra have been scaled to the same intensity at 400 nm.

will require a variable-temperature and variable-field magnetic circular dichroism (VTVH-MCD) investigation, which is planned. At present, however, we will simply use the assignment by Schultz and co-workers of the shoulder that extends into the visible region as a d−d transition, $^3T_{1g} \rightarrow {}^3E_g$ ($\approx 10Dq$) in O_h symmetry.[13,57] The consequence of this assignment will be discussed in the LFT section below.

Magnetometry. Schultz and co-workers measured the room-temperature magnetic moment of $[Tp_2Mn]^+$ and $[Tp^*_2Mn]^+$ in 1,2-dichloroethane[57] and in CD_3CN solutions (DMF-d_7 for $[Tp^*_2Mn]^+$).[13] In the original study, $\mu_{eff} = 3.2$ was reported for both complexes,[57] whereas in the later study, $[Tp^*_2Mn]^+$ appeared to exhibit a slightly higher room-temperature moment ($\mu_{eff} \approx 3.6$–3.7, based on their Figure 1).[13] These solution values are not consistent with $S = 1$ (spin-only $\mu_{eff} = 2.83$ vs 4.90 for $S = 2$); using $g = 2.00$ would give "S" = 1.42, i.e., midway between $S = 1$ and 2, or, alternatively, $g = 2.62$ results for $S = 1$ ($g = 1.51$ for $S = 2$). We found here $\mu_{eff} = 2.3$ for **3b** in CH_3CN solution (Evans method). As with the tris(pyrazolyl)borate complexes, this value is more consistent with $S = 1$ than any other spin-only option, but not ideally so: it gives "S" = 0.75 for $g = 2.00$ or $g = 1.6$ for $S = 1$. Thus, the room-temperature magnetic moment of each of the three complexes in solution is puzzling and suggestive of either significant orbital contributions or possibly spin-crossover behavior, which has been seen experimentally for six-coordinate Mn(III),[61−63] and recently studied theoretically.[63−65]

As mentioned above, we are at present focusing on understanding the solid-state electronic properties of these complexes. We have, therefore, measured the powder dc susceptibility of **1**, **2**, and **3a**, over the temperature range of 2–300 K. In striking contrast to the solution magnetometry, for both tris(pyrazolyl)borate complexes, there was no difficulty in describing the magnetic data by a spin-only model of $S = 1$ incorporating axial zfs, reasonable g values, and with no evidence for spin-crossover behavior in the solid state.

For compound **1**, the high-temperature ($T > 50$ K) average value of $\mu_{eff} = 2.68(1)$ matches the expected spin-only value with $g = 1.90$, a reasonable g value for a less than half-filled d shell ion ($g < 2.00$). The complete magnetic data were fitted to an $S = 1$ spin Hamiltonian model, as given in eq 1, but with axial symmetry ($E = 0$) and with isotropic g ($\beta_e g B \cdot \hat{S}$). With $D > 0$, the fit was excellent. The quality of the fit meant that further refinement, such as inclusion of temperature-independent paramagnetism (TIP) and/or use of rhombic zfs and/or axial g values, led to no significant changes in the D and g_{avg} values, and indeed incorporating such terms may amount to overparameterization. The data and this fit are shown in Figure 3 (top) as χT versus T. The fit parameters are summarized in

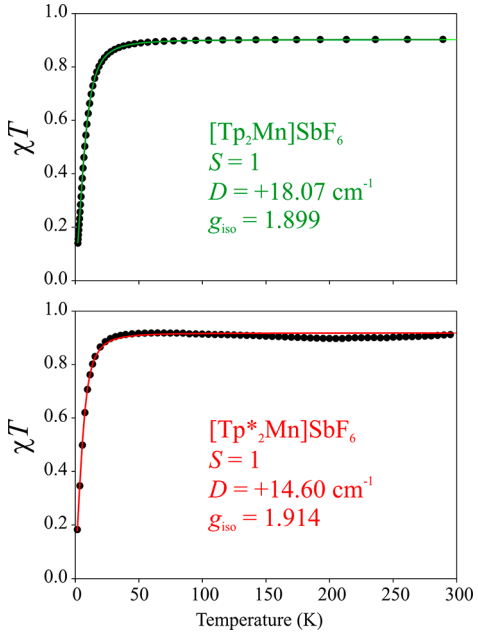

Figure 3. dc magnetic susceptibility of powder $[Tp_2Mn]SbF_6$ (**1**, top) and $[Tp^*_2Mn]SbF_6$ (**2**, bottom), each measured at an external field of 1 kOe. Experimental points are shown along with the fit of each using a spin Hamiltonian with the parameters as shown. Inclusion of TIP had essentially no effect on the fits. Fits using a negative value for D were unsuccessful in both complexes.

Table 2. In contrast, fits using $D < 0$ were unsuccessful, failing to converge and/or yielding unreasonable parameters. This confidence in determination of the (positive) sign of D is atypical from magnetometry, yet is corroborated by HFEPR, as discussed below.

The results for **2** were qualitatively the same, as seen in Figure 3 (bottom), with $\mu_{eff} = 2.69(1)$ at high temperature. The data are likewise easily fitted to an $S = 1$ spin Hamiltonian with $D > 0$ (and $g_{iso} = 1.91$), with no need for inclusion of rhombic zfs, g anisotropy, or TIP. The fit parameters are given in Table 2. As with **1**, fits using $D < 0$ were unsuccessful.

Complex **3a** was also investigated by powder dc susceptibility, and its behavior was quite different from that of **1** and **2**. The drop in χT occurs at much higher temperature, and fits yield a large magnitude D (~ 50 cm^{-1}) that also required a small rhombic component ($|E/D| \approx 0.04$). Use of axial g values or TIP had only minor effects on the fit, although use of axial g without TIP fit the data essentially perfectly. The data and best fits are shown in Figure 4 (see also Table 2). More surprisingly, fits only with $D < 0$ were successful in this case so that the spin ground state for **3a** is $|S, M_S\rangle = |1, \pm 1\rangle$. These results from magnetometry are indirectly confirmed by HFEPR, as discussed below.

HFEPR. Single-frequency spectra of **1** and **2** at low temperatures are shown in Figure 5. The spectra are

dx.doi.org/10.1021/ic301630d | Inorg. Chem. 2013, 52, 144−159

Table 2. Spin Hamiltonian Parameters for Mn(III) Scorpionate Complexes, $[L_2Mn]^+$ (L = Tp^-, Tp^{*-}, $PhB(MeIm)_3^-$), Determined by HFEPR, FD-FT THz-EPR, and Magnetometry

	D (cm^{-1})[d]	E (cm^{-1})[e]	g_x	g_y	g_z[f]
		$[Tp_2Mn]SbF_6$ (**1**)			
HFEPR	+17.97(1)	0.42(2)	2.065(6)	2.073(8)	1.978(6)
magnetometry[a]	+18.07				1.899
FD-FT THz-EPR[b]	17.874(5)	0.420(5)			
		$[Tp^*_2Mn]SbF_6$ (**2**)			
HFEPR	+15.89(2)	0.04(1)	2.079(7)	2.074(6)	2.075(15)
magnetometry[a]	+14.60				1.914
		$[\{(PhB(MeIm)_3\}_2Mn]CF_3SO_3$ (**3a**)			
HFEPR[c]					
magnetometry[a]	−49.9	−2.0	2.26		2.14

[a]Fits to the variable-temperature dc susceptibility for **1** were perfect when employing only an axial zfs and isotropic g value (given here arbitrarily as g_z). No TIP was necessary, and inclusion of rhombic zfs and/or axial g values was deemed as leading to overparameterization. Fits to the data for **3a** required a slightly rhombic zfs and were best with an axial g value (given here arbitrarily as g_x ($g_\perp$) and g_z ($g_\parallel$)); inclusion of TIP had little effect. [b]Only **1** was investigated by this technique, which provides zfs parameters, but does not provide g values quantitatively; however, application of an external magnetic field led to splittings of the frequency-domain transitions, consistent with the g values determined quantitatively from field-domain HFEPR (see Figure 7). [c]HFEPR spectra were not observed. [d]The sign of D has been determined in each complex and is thus explicitly given. [e]The sign of E is assigned to that of D, by convention. [f]The isotropic g value determined for **2** by magnetometry is arbitrarily listed as g_z.

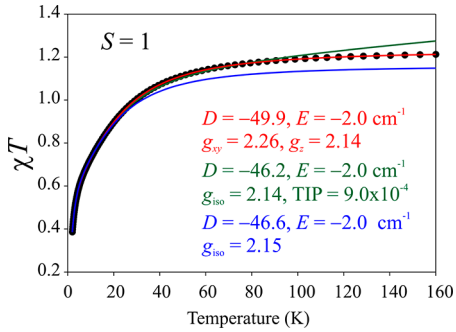

Figure 4. dc magnetic susceptibility of powder $[\{PhB(MeIm)_3\}_2Mn](CF_3SO_3)$ (**3a**) measured at an external field of 1 kOe. Experimental points are shown along with fits using a spin Hamiltonian with the parameters as shown. Fits using a positive value for D were unsuccessful, regardless of inclusion of TIP and/or axial g values.

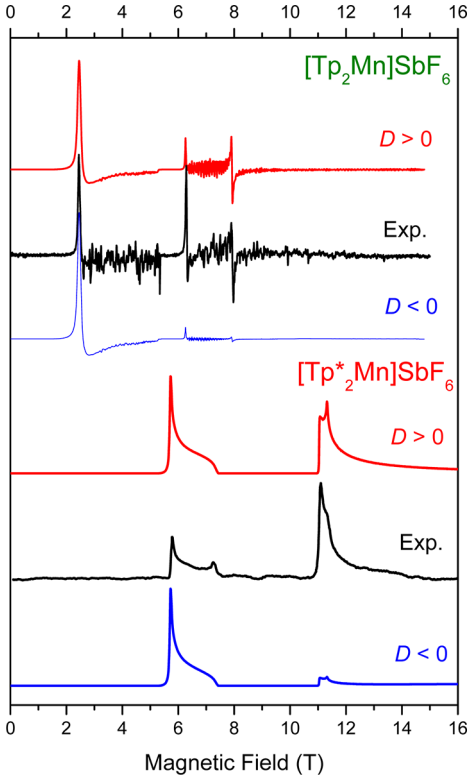

Figure 5. HFEPR spectra of $[Tp_2Mn]SbF_6$ (**1**, upper black trace) and $[Tp^*_2Mn]SbF_6$ (**2**, lower black trace), with simulations. Experimental conditions: (**1**) temperature, 2.0 K; frequency, 604 GHz; magnetic field modulation at 310 Hz; (**2**) temperature, 4.2 K; frequency, 642 GHz; optical modulation at 250 Hz. Simulation parameters: (**1**) $|D|$ = 17.67 cm^{-1}, $|E|$ = 0.46 cm^{-1}, $g_{x,y}$ = 2.12, g_z = 2.1; (**2**) $|D|$ = 15.80 cm^{-1}, $|E|$ = 0.09 cm^{-1}, g = 2.1 (isotropic). Red traces correspond to positive D values while blue traces correspond to negative ones. By convention, E is assigned the same sign as D.

accompanied by respective powder-pattern simulations, the latter determined with the spin Hamiltonian parameters provided in the caption. Generally, they can be interpreted as originating from a triplet (S = 1) spin state characterized by large zfs, on the order of $|D| \sim 16-18$ cm^{-1}. The field-modulated spectrum of **1** is close to a powder pattern; however, because of the small single-crystal line width and the resolution power inherent to magnetic modulation, one can notice the characteristic "quasi noise" due to a finite number of crystallites in the sample, and the spread of resonances over a wide field range.[27] This "quasi noise" could be partly digitally reproduced in the simulations by reducing the number of points used to construct the powder pattern (upper colored traces). The simulations also allowed us to determine the sign of D, which is positive (the $|S, M_S\rangle = |1, 0\rangle$ spin sublevel having a lower energy than the $|1, \pm1\rangle$ sublevels). This result is in agreement with magnetic susceptibility, and moreover, the magnitude of D is in close agreement (differing by only 0.5%) between the two techniques. We have frequently experienced difficulty in reconciling magnetometry quantitatively with HFEPR,[66,67] so the agreement here for **1** is extremely gratifying and leads to complete confidence in the result.

The "quasi-noise" is not as pronounced for complex **2**, whose spectrum (Figure 5, lower part) was recorded using optical modulation (chopping the sub-millimeter wave beam), yet that spectrum is not an ideal powder pattern, either. However, the correspondence to a simulation with positive D allowed attributing a positive value to this complex as well, again in

dx.doi.org/10.1021/ic301630d | Inorg. Chem. 2013, 52, 144−159

agreement with magnetic susceptibility. The difference in D for **2** between the two techniques is ~8%, which is still quite good.

To obtain an accurate, frequency-independent set of spin Hamiltonian parameters, we performed a tunable-frequency EPR experiment, where frequency is varied in relatively small steps, and a spectrum taken at each frequency. The observed turning points are collected as a 2D data set of resonance fields versus frequency, and spin Hamiltonian parameters fitted to the complete data set.[68] The results are shown in Figure 6. Squares

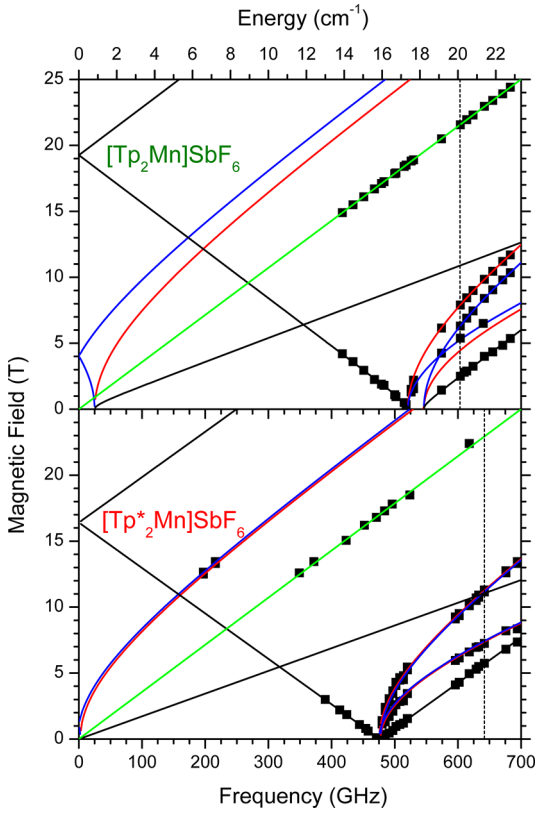

Figure 6. 2D field/frequency (or quantum energy) maps of HFEPR turning points for complexes $[Tp_2Mn]SbF_6$ (**1**, upper diagram) and $[Tp^*_2Mn]SbF_6$ (**2**, lower diagram). The squares are experimental points, and the curves were simulated using best-fit spin Hamiltonian parameters, as in Table 2. Red curves denote turning points with $B_0 \| x$, blue curves with $B_0 \| y$, black curves with $B_0 \| z$, while the green lines correspond to a $g = 2$ impurity, most probably Mn(II) (outside the field range shown in Figure 5). The vertical broken lines indicate the frequencies at which each spectrum in Figure 5 was collected. The data set corresponds to $T = 4.5$ K.

are experimental turning points while curves were computed using best-fit spin Hamiltonian parameters, as in Table 2. It is apparent that there are at least two zero-field energy gaps in **1** (see FD-FT THZ-EPR section below), which means that its tensor is somewhat rhombic, although the rhombicity factor is small ($E/D \sim 0.02$). To the contrary, zfs of **2** is almost perfectly axial ($E/D \sim 0.002$) and its rhombicity is visible only by the slight doubling of the perpendicular turning points between 11.5 and 12 T acquired at frequencies of 197 and 216 GHz (spectra not shown, but represented by squares at the respective frequencies in Figure 5 (bottom)).

Complex **3b** was also investigated by HFEPR. No signals attributable to any $S = 1$ or $S = 2$ species were observed. The extreme air sensitivity of that complex necessitated the use of sealed quartz ampules as holders, which puts a limit to the practical frequency of about 400 GHz. However, even in these conditions, complexes **1** and **2** produce observable resonances, which leads to a conclusion that the zfs of **3b** is considerably larger than that of **1** and **2**.

FD-FT THz-EPR. Because of beamtime limitations, the similarity between the two tris(pyrazolyl)borate complexes, with **2** being nearly axial, and the difficulty of handling **3a** and **3b**, only complex **1** was investigated by FD-FT THz-EPR.[30] The present FD-FT THz-EPR (i.e., frequency domain) results confirmed the HFEPR (i.e., field domain) results for this complex. This is shown in Figure 7, which presents the FD-FT

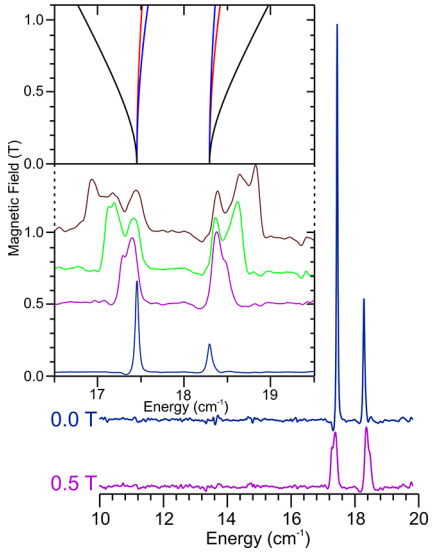

Figure 7. FD-FT THz-EPR spectrum of $[Tp_2Mn]SbF_6$ (**1**) as a PTFE pellet, recorded at 2 K, and at zero external magnetic field (navy blue trace) and at 0.5 T (violet trace). The relative intensities of the two traces are as observed (with integrated areas ca. 1:0.8). The two zero-field signals correspond to $|S, M_S\rangle = |1, 0\rangle \rightarrow |1, \pm 1\rangle$, with energies $\{|D| - |E|\}$, $\{|D| + |E|\}$. The inset shows an expansion of the region of interest with the further effect of the external magnetic field (0 T, navy blue trace; 0.50 T, violet; 0.75 T, green; 1.0 T, brown). The intensities of the traces in the inset are scaled for presentation purposes, and their baselines are each aligned with the ordinate value of their magnetic field of measurement. Above these experimental traces is a 2D map on the same scale of the EPR transitions, as in Figure 6 (red curves, turning points with $B_0 \| x$; blue with $B_0 \| y$; black with $B_0 \| z$). These curves are calculated as in Table 2, using the zfs parameters from FD-FT THz-EPR and the g values from HFEPR.

THz-EPR spectra recorded at zero field and at 0.5 T applied external field, with a spectrometer resolution of 0.04 cm^{-1}. We have found that, at this resolution, the EPR line width dominates the width of the observed resonance peaks. At zero field, there are two sharp resonances, respectively, at 17.45(4) and 18.29(4) cm^{-1}. Taking advantage of the HFEPR data, these signals can readily be assigned to the zero-field transitions $|S, M_S\rangle = |1, 0\rangle \rightarrow |1, \pm 1\rangle$, wherein the $M_S = \pm 1$ doublet is split by a small rhombic zfs component. The lower signal corresponds to $|D - E|$ and the higher, $|D + E|$ (E assigned the same sign as D), which yields $|D| = 17.87(4)$, $|E| = 0.42(4)$ cm^{-1}. This D value differs by 0.1 cm^{-1} from that determined by HFEPR, but it must be noted that, in the present HFEPR studies on **1**, zero-field resonances were not directly observed, but were obtained by fitting the 2D field-frequency map (Figure 7). Indeed, this discrepancy likely represents the limit of precision in

dx.doi.org/10.1021/ic301630d | Inorg. Chem. 2013, 52, 144−159

determination of zfs among different experimental techniques. Application of the magnetic field causes the separation between the two signals to increase and each to broaden and develop peaks. This is the consequence of the electronic Zeeman effect, which can be seen in the inset over the range of 0−1 T. The experimental spectra are compared to a 2D field-frequency map generated as in Figure 7. The spread of the pattern matches quite well with that predicted from the g values determined quantitatively by HFEPR. The origin of the specific shape of the pattern, however, is not known, as the features do not necessarily correspond to canonical turning points, unlike the field-domain HFEPR spectra.[69] Quantitative analysis of magnetic field effects in FD-FT THz-EPR of these and other systems is the subject of future studies.

LFT Analysis. Octahedral Mn(III) generally exhibits a high-spin (quintet) ground state, such as in $[MnF_6]^{3-}$,[70] Mn^{3+}-doped rutile,[71] $[Mn(H_2O)_6]^{3+}$,[14,72] and in the trigonally distorted octahedral complex $Mn(acac)_3$ (acac = anion of 2,4-pentanedione).[73] Strong-field ligands, however, can lead to a low-spin (triplet) ground state, such as in $[Mn(CN)_6]^{3-}$.[74,75] Other hexacoordinate Mn(III) complexes, between these two ligand strength extremes, by virtue of their N6 or N4O2 donor sets, can exhibit spin-crossover behavior.[61−63] It is, therefore, at first glance remarkable that Mn(III), when complexed by two scorpionate ligands (both pyrazole and imidazolyl carbene donors), exhibits a low-spin ground state in the solid state at all accessible temperatures. We, therefore, seek to rationalize this triplet ground state and simultaneously explain the zfs observed for **1** and **2**. We note that the zfs for the "traditional" (i.e., HS) hexacoordinate Mn(III) complexes is 4-fold smaller in magnitude and of opposite sign than that seen here for these Mn(III) spin triplets. For example, for $[Mn(H_2O)_6]^{3+}$, D = −4.514 cm^{-1},[14,72] and for $Mn(acac)_3$, D = −4.52 cm^{-1}.[73] It is also interesting that these complexes have essentially the same D values, despite one having neutral monodentate ligands and the other, anionic bidentate ligands. In contrast, we see here a roughly 25% difference in magnitude of D between complexes that differ only in pyrazolyl 3,5-position substituents. The effect on zfs of seemingly minor changes in pyrazolyl substituents has been also noted in a study of monoscorpionate Co(II) complexes (TpCoL, where L = various unidentate anionic ligands).[76] This result is perhaps a small manifestation of the electronic tunability of the scorpionate ligand, although how to play this tune is not yet clear.

Our LFT analysis is hindered by the lack of definitive assignment of d−d transitions. We can, however, look to a study on a Cr(III) ($3d^3$, S = 3/2) analogue, $[Tp_2Cr]ClO_4$, for which d−d electronic transitions are readily observed (by absorption, emission, and MCD spectroscopies).[38] We have done our own analysis of the data reported by Fujihara et al. using only their assignments of the $^4A_2(^4F) \rightarrow {}^4T_2(^4F)$ band at 21 800 cm^{-1} and the $^4A_2(^4F) \rightarrow {}^4T_1(^4P)$ band at 26 740 cm^{-1}. This allows determination of Dq = 2180 cm^{-1} and B = 444 cm^{-1} (48% of the free-ion value, based on B = 933 cm^{-1} for Cr^{3+}[33,36]) Considering the greater covalency in Mn(III) versus Cr(III), it is possible that the shoulder observed in solution at ∼400 nm in $[Tp_2Mn]^+$ and $[Tp^*_2Mn]^+$ could be assigned to a transition from t_2^4 to t_2^3e ($^3T_{1g} \rightarrow {}^3E_g$ in O_h symmetry) to give $Dq \approx$ 2580 and 2410 cm^{-1} in $[Tp_2Mn]^+$ and $[Tp^*_2Mn]^+$, respectively.[57] As discussed above, we are focusing at present only on the solid state, so the reflectance absorption data give for **1** and **2**, $Dq \approx$ 2160 and 2105 cm^{-1}, respectively.

We can also use the reduction in Racah parameters suggested by the Cr(III) study, which, in combination with the Racah parameters for free-ion Mn(III),[33,36] gives rough estimates for these values as $B \approx$ 450 cm^{-1}, $C \approx$ 1950 cm^{-1}. This crude model indeed gives a $^3T_{1g}(^3H;\ t_2^4)$ ground state (in O_h symmetry) with the "traditional" $^5E_g(^5D;\ t_2^3e)$ state roughly 14 000 cm^{-1} higher in energy for **1** and 12 000 cm^{-1} for **2** (due to its presumed lower Dq value). The spin quintet is within ∼9000−10 000 cm^{-1} of the triplet ground state for the two complexes. Use of Racah parameters that are more typical of coordination complexes (e.g., B = 670 cm^{-1}, C = 2900 cm^{-1}; ∼70% of the free-ion values for B and C) still give a triplet ground state for both complexes, although the quintet is much closer in energy, within ∼4000 cm^{-1} for both complexes. Singlet states are found in the range of ∼6000−9000 cm^{-1} above the triplet ground state, depending on which of the above parameter sets is used.

The next problem to address is the trigonal distortion away from O_h symmetry, as observed in the crystal structures, and its effect on the electronic structures of these complexes. This is best treated initially using the AOM, as was done by Fujihara et al. for $[Tp_2Cr]^+$.[38] The AOM we employ here defines the z axis along the 3-fold axis (the B−Mn−B angle is exactly 180°, due to the inversion center) and the x axis is defined along the B1(A)−N2(A) vector. The relevant metrical parameters are given in Tables S1−S3 (Supporting Information) and demonstrate the 3-fold axis with minimal twisting of the pyrazolyl ligands. For simplicity, we, therefore, define the six N ligands at $\phi = n\pi/3$, n = 0−5 for both complexes and at θ = 53.32° (180−θ for the opposite ligand) and 54.75° for $[Tp_2Mn]^+$ and $[Tp^*_2Mn]^+$, respectively; these are values equal or nearly equal to those for ideal geometry.[77]

The next consideration is the bonding parameters of the Mn−N interactions. Variation in Mn−N bond distances within each complex is minimal, and given the crude nature of the AOM used here, we treat all of the pyrazole N donors as equivalent, as was done for $[Tp_2Cr]^+$.[38] Given the relationship

$$\Delta = 10Dq = 3\varepsilon_\sigma - 2\varepsilon_{\pi\sigma} - 2\varepsilon_{\pi c}$$

we can estimate values for the bonding parameters by setting $\varepsilon_{\pi c} = 0$ and using the ratio $(\varepsilon_\sigma/\varepsilon_{\pi s}) \approx 6.4$, which is derived from the results of Fujihara et al.[38] This gives ε_σ = 9600, $\varepsilon_{\pi s}$ = 1500 and ε_σ = 8970, $\varepsilon_{\pi s}$ = 1400 (all in cm^{-1}), respectively, for $[Tp_2Mn]^+$ and $[Tp^*_2Mn]^+$.[78] This model then gives a trigonal splitting of the $^3T_{1g}$ state into a $^3A_2$ ground state and a ^3E excited state that is roughly 4600 cm^{-1} higher in energy for $[Tp_2Mn]^+$ (∼4200 cm^{-1} for $[Tp^*_2Mn]^+$).[79] The smaller bonding parameters derived from the solid-state reflectance spectra give trigonal splittings of roughly 3600−3900 cm^{-1} for the two complexes. There is a variety of triplet excited states in the energy range of 20 000−30 000 cm^{-1} (λ = 500−330 nm) above the ground state. The energy levels of these various $^3A_1$, $^3A_2$, and ^3E excited states depend on the complex and its specific model used (larger vs smaller Racah parameters); however, the energy levels for $[Tp^*_2Mn]^+$ are lower than those for $[Tp_2Mn]^+$. Note that $^3A_2 \rightarrow {}^3E$ is allowed in D_3 symmetry with x,y polarization and $^3A_2 \rightarrow {}^3A_1$ is allowed with z polarization, so the relatively high intensities, as well as the energies, of the proposed d−d electronic transitions can be rationalized by this simple model.

The program Ligfield also provides d orbital occupancies for each state. We describe these here also to emphasize the lately often ignored point,[80] which is that in trigonal symmetry there

dx.doi.org/10.1021/ic301630d | Inorg. Chem. 2013, 52, 144−159

Table 3. LFT Parameters (in cm^{-1}) for Mn(III) Scorpionate Complexes, $[L_2Mn]^+$ (L = Tp^-, Tp^{*-}, $PhB(MeIm)_3^-$), Estimated from Experimental Data

compound	Racah parameters: B, C[a]	bonding parameters: ε_σ, $\varepsilon_{\pi s}$[b] (Dq, Dt)[c]	spin–orbit coupling: ζ[a]	calculated D [exptl D][d]
$[Tp_2Mn]SbF_6$ (**1**)	450, 1950	8040, 1260[e]	290	+17.78
	670, 2900	″	330	+18.23
	450, 1950	(2160, 500)[c]	285	+18.32
	670, 2900	″	315	+17.72
				[+17.97]
$[Tp^*_2Mn]SbF_6$ (**2**)	450, 1950	7830, 1220[f]	285	+15.92
	670, 2900	″	315	+15.74
				[+15.89]
$[\{PhB(MeIm)_3\}_2Mn]CF_3SO_3$ (**3a**)	450, 1950	7500, 1100[f]	″	+29.6
	670, 2900	″	350[h]	+22.7
	450, 1950	12500, 0[g]	″	[j]
	670, 2900	″	300[i]	146[k]
			″	[−50]

[a]The free-ion parameters for Mn^{3+} are B = 950 cm^{-1}, C = 4112 cm^{-1} (C = 4.33B),[36] and ζ = 351 cm^{-1}.[34] We employ two choices of Racah parameters: the first listed is based on results for $[Tp_2Cr]^+$,[38] and the second is chosen as ∼70% of the free-ion values as being more typically representative for coordination complexes. Intervals of 5 cm^{-1} were used to adjust ζ; use of higher precision is gratifying in terms of matching experiment, but meaningless given the uncertainties in all of the other parameters. [b]AOM bonding parameters based, in general, on $\varepsilon_{\pi s} \equiv \varepsilon_\sigma/6.4$ and $\varepsilon_{\pi c} \equiv 0$, as proposed by Fujihara et al. for $[Tp_2Cr]^+$.[38] [c]Crystal-field parameters based on Dq value from reflectance data with trigonal splitting chosen to be comparable with AOM value. This model was applied only to **1**, for illustrative purposes. [d]From HFEPR (for **1** and **2**); from magnetometry (for **3a**). Rhombic zfs, E, is not given here, and no attempt was made to reproduce this small effect by calculations. The value from magnetometry for **3a** may not be meaningful as an S = 1 spin Hamiltonian may not be appropriate in this case (see text). [e]Based specifically on the assignment as a d–d band of the electronic absorption shoulder observed here in diffuse reflectance spectra at 460–465 and 475 nm, in **1** and **2**, respectively. [f]Based specifically on the assignment as a d–d band of the electronic absorption shoulder observed here in diffuse reflectance spectra at 515–565 nm in **3b**. [g]This AOM ignores π-bonding, but uses a much larger σ-bonding parameter, as suggested by work on Ni(II) complexes with this type of tris(carbene) ligand.[10] This model gives effectively a $^3T_1$ ground state with unquenched orbital angular momentum. [h]This value for ζ was used simply to correspond with the uppermost end of the range used for **1** and **2**, for which the zfs was well-determined (by HFEPR) and for which an S = 1 spin Hamiltonian is appropriate. [i]This value for ζ was used simply to correspond with the lower end of the range used for **1** and **2** for which the zfs was well-determined (by HFEPR) and for which an S = 1 spin Hamiltonian is appropriate. [j]The lowest energy states are not a spin singlet and a spin doublet, so an S = 1 model cannot be applied (see Table S4 (Supporting Information) for energy levels and further information). [k]The lowest energy states are a spin singlet and a spin doublet, so an S = 1 model can be applied (see Table S4 (Supporting Information) for energy levels and further information).

are no distinct d_{xy} and $d_{x^2-y^2}$ or d_{xz} and d_{yz} orbitals, but each pair is totally mixed. However, we will use these orbital designations due to their familiarity rather than, respectively, (M_L = ±2) and (M_L = ±1). In the trigonal symmetry case of $[Tp_2Mn]^+$ and $[Tp^*_2Mn]^+$, the d_{z^2} orbital is the lowest in energy, d_{xy} and $d_{x^2-y^2}$ are next, and d_{xz} and d_{yz} are the highest. The $^3A_2$ ground state can be described approximately as $d_{z^2}^{2(\pm)}(d_{x^2-y^2},d_{xy})^{1.5(++)}$-$(d_{xz},d_{yz})^{0.5(+)}$, where the superscripts refer to the (whole or fractional, as appropriate) spins for the M_S = +1 state. The ^3E first excited state can be described approximately as $d_{z^2}^{1(+)}$-$(d_{x^2-y^2},d_{xy})^{2(+-)}(d_{xz},d_{yz})^{1(+)}$. For comparison, the $^5E_{(g)}$ state, which is the ground state in a weaker field trigonal complex, such as $Mn(acac)_3$, here corresponds to $d_{z^2}^{1(+)}(d_{x^2-y^2},d_{xy})^{1.7(++)}$-$(d_{xz},d_{yz})^{1.3(++)}$ and the $^5T_{1g}$ excited state in O_h symmetry splits into (for M_S = +2) ^5E (corresponding to $d_{z^2}^{1(+)}(d_{x^2-y^2},d_{xy})^{1.3(++)}$-$(d_{xz},d_{yz})^{1.7(++)}$) and $^5A_1$ (corresponding to $d_{z^2}^{0}(d_{x^2-y^2},d_{xy})^{2(++)}(d_{xz},d_{yz})^{2(++)}$). For the other models, the orbital occupancies vary slightly, but the overall picture is the same.

Spin–orbit coupling can then be introduced to cause zfs within these states. The value for ζ required to match experiment depends on the specific complex and the model used (larger vs smaller Racah parameters); however, the range is fairly narrow, within ∼10% of 310 cm^{-1}, which itself is ∼90% of the free-ion value. The lower end of the range is appropriate for the smaller Racah parameters, which are based on experiment for Cr(III), while the larger values are more for test purposes. The results are summarized in Table 3. This model does not consider spin–spin coupling (SSC), which might well be significant in these systems, as has been found elsewhere.[67,81−85] QCT calculations (vide infra) suggest that contribution of SSC to zfs is small relative to SOC, but not insignificant and is in the same direction as SOC (i.e., $D^{SOC} > D^{SSC} > 0$). The contribution of D^{SSC} would effectively reduce the value of ζ needed for SOC calculations. Nevertheless, it is possible to reproduce, using reasonable LFT parameters and approximations, the sign and magnitude of zfs observed in these complexes. We have not seriously attempted to reproduce the very small rhombic splitting ($|E/D|$ = 0.02, 0.002 for **1** and **2**, respectively) that is observed in these complexes; this could be obtained in a myriad of ways, such as the use of the real angles (see Tables S2 and S3, Supporting Information), or having slight differences in bonding parameters among the N6 donor set.[86]

We conclude with the crystal-field model for illustrative purposes. We apply this model to $[Tp_2Mn]^+$ and use the value for cubic splitting, Dq = 2160 cm^{-1}. Inclusion of trigonal splitting defined by Dt = 500 cm^{-1} gives a $^3A_2$ ground state with ^3E lying 3500–3600 cm^{-1} higher in energy, roughly comparable to the AOM. Inclusion of SOC similar in magnitude to that used above for the AOM also gives zfs in good agreement with experiment (see Table 3). What is useful about the crystal-field model is that it is easy to swap the ground and first excited state simply by a change in sign of the distortion parameter. Use of Dt = −500 cm^{-1} thus gives a ^3E ground state and $^3A_2$ first excited state. Inclusion of SOC (ζ = 300 cm^{-1}, as before, with

dx.doi.org/10.1021/ic301630d | Inorg. Chem. 2013, 52, 144–159

either choice of Racah parameters), however, gives behavior that can in no way be modeled by a spin Hamiltonian with S = 1. The six lowest energy states derived from ^{3}E comprise a singlet ground state with no spin ($\langle S_z^2 \rangle \approx 0$), a first excited singlet with no spin at ~45 cm^{-1}, a next excited doublet with almost no spin ($\langle S_z^2 \rangle \approx \pm 0.0003$) at ~160 cm^{-1}, and a highest, magnetic doublet at ~300 cm^{-1} ($\langle S_z^2 \rangle \approx \pm 0.7$). Such an effectively nonmagnetic system would give no HFEPR spectra. It is clear that, in **1** and **2**, the electronic ground state is ^{3}A$_2$ (from ^{3}T$_{1g}$ in O_h, from primarily free-ion ^{3}H), which allows successful application of an S = 1 spin Hamiltonian. The difficulty of dealing with bis(scorpionate) complexes for which the ground states are indeed orbitally degenerate has been recently shown by Myers et al.,[12] for the case of [Tp$^{R,R'}{}_2$Co] (where the ground state is ^{4}E$_{(g)}$ from ^{3}T$_{1g}$ in O_h, from free-ion ^{4}F). As we discuss next, this situation may well be appropriate for [{PhB(MeIm)$_3$}$_2$Mn]$^+$.

For complexes **3a** and **3b**, the lack of HFEPR data precludes an analysis, as detailed as above, yet this experimental failure may be significant. At the outset, the structural data for **3a** suggest that the same AOM description can be employed as for the tris(pyrazolyl)borates. As seen in Tables S1−S3 (Supporting Information), this complex shows almost ideal trigonal symmetry. The presence of two crystallographically independent molecules per asymmetric unit is a minor complication as the differences in the θ angles is minor and we shall use an average of all six (θ = 52.48°), along with idealized ϕ angles. The bonding parameters for the imidazolyl carbon donors are even less established than for pyrazolyl nitrogen donors.

By analogy with the method applied to the tris(pyrazolyl)-borate complexes, we can use the reflectance UV−vis spectrum of **3a** for which the center of the lowest energy band gives an estimate of 10Dq = 18 550 cm^{-1}. Following the same procedure as described above, we can derive bonding parameters consistent with this value and obtain the results given in Table 3 for both the higher and the lower choices of Racah parameters. This model yields D in the range of 23−30 cm^{-1}, not dramatically different from the two tris(pyrazolyl)borate complexes, and potentially observable by HFEPR at the highest range of available frequencies.

Clearly, another approach is needed for this unusual ligand. In a study of a Ni(II) complex with a closely related ligand, HB(^{t}BuIm)$_3$NiBr, values of ε_σ = 6600 cm^{-1} were proposed, compared to 5160 cm^{-1} for the analogue, Tp*NiBr.[10] The study also explored π-bonding in these complexes, but we will disregard that possibility in the present case. This means that the tris(carbene)borate ligand could be considered as roughly a 30% stronger σ-donor than the typical tris(pyrazolyl)borate scorpionate ligand. We can use this crude approximation as well, so that $\varepsilon_\sigma \approx$ 12,500 cm^{-1}. We maintain the two choices of Racah parameters, which cover all realistic scenarios. This AOM of very strong σ-bonding and no π-bonding gives an electronic ground state in the absence of SOC that is very nearly ^{3}T$_1$ (O symmetry). There is a ^{3}A$_2$ ground state, but the ^{3}E excited state is very close in energy (~100 cm^{-1} for the larger choice of Racah parameters and only 8 cm^{-1} for the smaller). As a result of this unquenched orbital angular momentum, application of SOC gives these nine lowest states at energies dominated by this interaction (i.e., roughly first-order energies for $J = L + S = 1$). For the choice of larger Racah parameters, the ground state is a nonmagnetic singlet (A$_1$ in O* and D_3*); there are singlet and doublet excited states at roughly $\zeta/2$ (T$_1$ in O*; A$_2$ and E in D_3*), and a singlet and two doublet higher excited states at roughly $3\zeta/2$ (T$_2$ and E in O*; A$_1$ and 2 × E in D_3*). The exact energies of these states and relevant higher energy electronic states are given in Table S5 (Supporting Information) for both choices of Racah parameters. The electronic structure of this model would give no observable HFEPR at sub-THz frequencies, and the magnetic behavior would be ill-suited for modeling using a spin Hamiltonian. Given the nonmagnetic ground state and relatively (in magnetic terms) high-energy nearest excited states, it is possible that even trace amounts of the spin quartet Mn(IV) oxidation product could have a disproportionate effect on the observed magnetic behavior.

QCT Analysis. DFT and UHF methods employing the program ORCA[39] were also used to probe the electronic structure of the complexes. These complexes are relatively large (even ignoring the counteranion) and present a challenge for computational methods. All three Mn(III) complexes were subjected to full DFT geometry optimization and were converged to the S = 1 state. Electronic structures were calculated by DFT both for the optimized geometries and for the crystallographically determined structures; only the latter structures were used for UHF calculations. A representative ORCA program input/output file using DFT is given in Table S6 (Supporting Information).

Compared to their crystallographic counterparts, the structures of the optimized complexes show only minor structural changes (Table 4). For example, in all cases, the Mn−ligand bonds elongate slightly (0.02−0.03 Å). Angles between metal−ligand bonds are changed by <1° in all compounds. The structural changes are smallest for the sterically unencumbered [Tp$_2$Mn]$^+$ cation.

Table 4. Selected Metric Parameters (Bond Distances in Å; Bond Angles in deg) for Geometry-Optimized Mn(III) Scorpionate Complexes [L$_2$Mn]$^+$ (L = Tp$^-$, Tp*$^-$, PhB(MeIm)$_3^-$) Using the BP Functional and TZVP/SVP Basis Sets; for Comparison, Corresponding Crystallographic Parameters for 1, 2, and 3a are Included in Parentheses

[Tp$_2$Mn]$^+$	
Mn−N(1)	1.999 (1.979)
Mn−N(2)	2.000 (1.988)
Mn−N(3)	2.000 (1.983)
N(1)−Mn−N(2)	88.22 (87.41)
N(1)−Mn−N(3)	88.30 (88.73)
N(2)−Mn−N(3)	88.23 (87.78)
[Tp*$_2$Mn]$^+$	
Mn−N(1)	2.023 (1.992)
Mn−N(2)	2.024 (1.998)
Mn−N(3)	2.024 (1.999)
N(1)−Mn−N(2)	89.63 (89.75)
N(1)−Mn−N(3)	89.63 (90.49)
N(2)−Mn−N(3)	89.58 (89.81)
[{PhB(MeIm)$_3$}$_2$Mn]$^+$	
Mn−C(45)	2.037 (2.014)
Mn−C(33)	2.051 (2.028)
Mn−C(20)	2.054 (2.037)
C(45)′−Mn(1)−C(33)	86.95 (86.96)
C(45)′−Mn(1)−C(20)	87.06 (87.29)
C(33)−Mn(1)−C(20)	85.79 (85.80)

The first property to be addressed is the relative stability of the spin triplet state. These results are summarized in Table 5.

dx.doi.org/10.1021/ic301630d | Inorg. Chem. 2013, 52, 144−159

Table 5. QCT Computational Results Using DFT for Mn(III) Scorpionate Complexes, $[L_2Mn]^+$ (L = Tp^-, Tp^{*-}, $PhB(MeIm)_3^-$): Calculated Spin Singlet−Triplet−Quintet Difference Energies and Calculated zfs (All Energies in cm^{-1}) and *g* Value Matrices for Triplet and Quintet States. Results Using Crystallographically Determined Geometries and Those from DFT-Optimized Geometries Are Given

complex	(singlet, quintet) − triplet[a]	*D*, |*E*|	g
$[Tp_2Mn]^+$, crystallographic geometry[b]			
S = 2	+8630	+71.71,[e] 2.95	[1.9958, 1.9983, 2.0075]
S = 1	0	+10.782, 0.042	[1.9865, 2.0264, 2.0290]
S = 0	+5350	NA	NA
$[Tp_2Mn]^+$, DFT-optimized geometry			
S = 2	+7564	−23.39,[e] 6.35	[1.9940, 1.9958, 2.0026]
S = 1	0	+10.291, 0.0015	[1.9848, 2.0256, 2.0257]
S = 0	+3951	NA	NA
$[Tp^*_2Mn]^+$, crystallographic geometry[c]			
S = 2	+7780	−81.33,[e] 9.82	[1.9938, 1.9964, 2.0028]
S = 1	0	+9.418, 0.016	[1.9839, 2.0262, 2.0274]
S = 0	+4000	NA	NA
$[Tp^*_2Mn]^+$, DFT-optimized geometry[a]			
S = 2	+756	+1.682, 0.023	[1.9928, 2.0143, 2.0147]
S = 1	0	+9.589, 0.0018	[1.9829, 2.0250, 2.0263]
S = 0	+13 496	NA	NA
$[\{PhB(MeIm)_3\}_2Mn]^+$, crystallographic geometry[d]			
S = 2	+15 400	−0.6924, 0.074	[1.9991, 1.9998, 2.0021]
S = 1	0	+8.260,[f] 0.371	[1.9964, 2.0706, 2.0806]
S = 0	+4330	NA	NA
$[\{PhB(MeIm)_3\}_2Mn]^+$, DFT-optimized geometry			
S = 2	+13 698	−0.9023, 0.064	[1.9989, 1.9996, 2.0021]
S = 1	0	+11.030,[f] 0.0584	[1.9939, 2.0670, 2.0802]
S = 0	+11 364	NA	NA

[a]The triplet state energy is defined as zero for ease of comparison among states. [b]Crystallographic geometry used for SbF_6^- salt (**1**, CSD code: PIBMUJ[13]) using a coordinate system defined for trigonal symmetry. [c]Crystallographic geometry used for SbF_6^- salt (**2**, CSD code: PIBNAQ[13]) using a coordinate system defined for trigonal symmetry. [d]Crystallographic geometry used for $CF_3SO_3^-$ (triflate) salt (**3a**, this work) using a coordinate system defined for trigonal symmetry. [e]This calculated zfs is surprisingly large in magnitude, given that "typical" octahedral Mn(III) complexes have much smaller magnitude values (e.g., $D = -4.52$ cm^{-1} for $Mn(acac)_3$[73]), which has been well-described by theory.[51,92] [f]This calculated zfs is surprisingly small, given that such a value should readily give HFEPR spectra, which were not observed, nor were magnetic measurements consistent with this small a zfs.

The DFT calculations properly predict that the spin triplet ground state is lower in energy for $[Tp_2Mn]^+$, by 1.0702 eV (8630 cm^{-1}) relative to the spin quintet based on crystallographic geometry. This value is smaller than that from LFT (11 000−12 000 cm^{-1}, depending on the specific AOM), but not vastly different. For $[Tp^*_2Mn]^+$, the spin-state energies are similar, but both singlet and quintet states are calculated to be closer in energy to the triplet than in $[Tp_2Mn]^+$, which is not consistent with either a stronger or a weaker ligand field for Tp^{*-} versus Tp^-. For $[\{PhB(MeIm)_3\}_2Mn]^+$, the triplet is again the ground state, but the singlet is lower and the quintet much higher in energy than in $[Tp_2Mn]^+$ and $[Tp^*_2Mn]^+$, which is consistent with a stronger ligand field for the tris(carbene)borate ligand than for the tris(pyrazolyl)borate.

The relatively minor structural perturbations that result from geometry optimization by DFT have a notable impact on the relative energies of the three spin states (Table 5). For each optimized model, the quintet spin state is relatively more stable than that calculated using the crystallographic geometry. This stabilization is most dramatic for $[Tp^*_2Mn]^+$, where the quintet spin state is now predicted to be only 756 cm^{-1} above the triplet and the singlet 13 496 cm^{-1} above. Thus, relative to the triplet state of $[Tp_2Mn]^+$, the corresponding quintet state is stabilized by ∼7000 cm^{-1} and the singlet destabilized by ∼9500 cm^{-1} as a result of the geometry optimization by DFT. We attribute this change to the elongation of Mn−ligand bonds in the optimized models, which would preferentially stabilize the higher spin states. However, it is somewhat surprising that this relatively minor change in bond lengths has such a dramatic impact on the relative energies of the quintet and singlet states. Nevertheless, the DFT energies for this series of complexes are overall quite acceptable, especially considering that accurate treatment of high-spin/low-spin energies remains a challenge even for hybrid functionals.[87,88]

The UHF calculations (Table S4, Supporting Information), on the other hand, predict the quintet spin state to be at lowest energy for $[Tp_2Mn]^+$ and $[Tp^*_2Mn]^+$ and only 1000 cm^{-1} above the triplet state for $[\{PhB(MeIm)_3\}_2Mn]^+$, representing a serious failure. It has been documented that pure Hartree−Fock methods grossly favor high-spin states due to the poor treatment of electron correlation,[89] and the present study fully validates this point.

The graphic ability of QCT calculations can also be taken to our advantage. Figure 8 presents the frontier molecular orbitals (FMOs), as quasi-restricted MOs (QROs), calculated by DFT for $[Tp_2Mn]^+$ with $S = 1$. These FMOs are all nearly purely metal-based, as seen in the figure. The highest doubly occupied MO (DOMO; QRO #121) corresponds to Mn $3d_{z^2}$ and the two semioccupied MOs (SOMOs; QROs #122, 123), which are nearly degenerate (calculated energy separation < 50 cm^{-1}), correspond to Mn $3d_{xy,x^2-y^2}$(noting that these are mixed with $3d_{xz,yz}$ in trigonal symmetry). This FMO occupancy

dx.doi.org/10.1021/ic301630d | Inorg. Chem. 2013, 52, 144−159

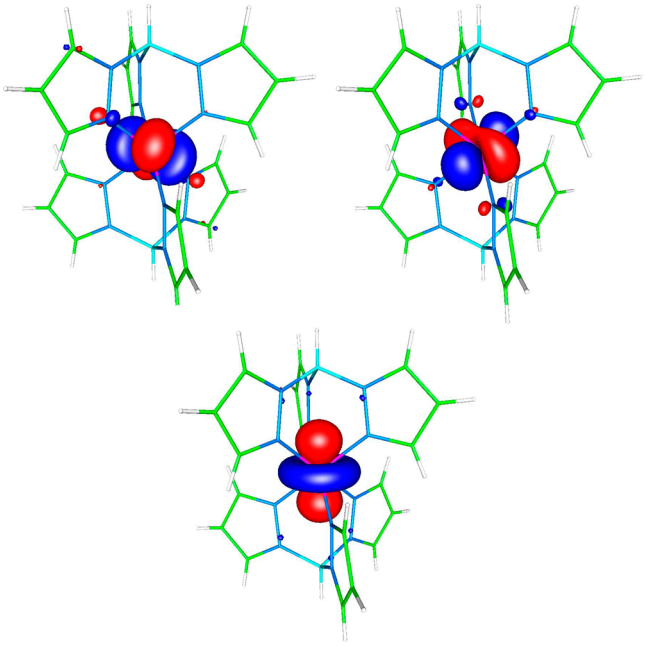

Figure 8. Highest occupied quasi-restricted MOs (QROs) calculated by DFT for $[Tp_2Mn]^+$ and plotted at the cutoff level (isodensity) of 0.04 using the software gOpenMol.[52,53] The bottom QRO is #121, at an energy level of −9.525 eV; the one at the upper right is #122, at −8.235 eV; and the one at the upper left is #123, at −8.229 eV. QRO #121 corresponds to the filled Mn $3d_{z^2}$ MO, and the essentially degenerate QROs #122 and #123 correspond to the half-filled Mn $3d_{xy,x^2-y^2}$ MOs (noting that these are mixed with $3d_{xz,yz}$ due to the trigonal symmetry). The other two Mn 3d-based MOs and the highest-energy ligand-based MO are shown in Figure S2 (Supporting Information).

$(d_{z^2}{}^2 d_{xy,x^2-y^2}{}^2)$ is qualitatively in complete agreement with that determined by LFT (see above). The second highest DOMO (QRO #120; shown in Figure S2, Supporting Information) is purely ligand-based, and corresponds to pyrazole π^* MOs. The FMO diagram (and LFT calculations) also suggest another, more important consequence, which is that the spin singlet would be orbitally degenerate (either QRO #122 or #123 would be a DOMO), as would be the spin quintet (either QRO #124 or #125, shown in Figure S2, which are separated in energy by only ∼350 cm^{-1}, would be a SOMO, rather than the LUMO for $S = 1$). Standard DFT methods are not suitable for cases of orbital degeneracy,[50,81,90] hence the failure of this single determinant method for the spin singlet, and likely for the quintet as well.

The program ORCA can also calculate spin Hamiltonian parameters[50,91] and has been successfully used for understanding zfs parameters for six-coordinate Mn(III) centers with $S = 2$ ground states.[51,92] Beginning with the crystallographically determined values and concerning only the zfs for $S = 1$ states, the values $D = +10.78$ cm^{-1}, $E = 0.04$ cm^{-1} resulted for $[Tp_2Mn]^+$, and $D = +9.42$ cm^{-1}, $E = 0.02$ cm^{-1} for $[Tp^*{}_2Mn]^+$ from the DFT computations. These zfs values have the correct sign and axial character, although more ideally axial than is the case for $[Tp_2Mn]^+$. The magnitude of D is too low by ∼40% in both cases, but this is not embarrassing given the difficulty of the system. More importantly, the ordering is correct: the D value for $[Tp_2Mn]^+$ is greater than that for $[Tp^*{}_2Mn]^+$, and proportionally the same as in experiment.[93] The calculated g values for $S = 1$ of $[Tp_2Mn]^+$, $g_\perp \approx 2.028$, $g_\parallel = 1.986$ (see Table 4) agree quite well with experiment: $g_\perp \approx 2.069$, $g_\parallel = 1.978$ (Table 2).

The calculated zfs parameters are also affected by the change in geometry between the crystallographic and DFT-geometry-optimized models (Table 5). This impact is reassuringly quite minor for the $[Tp_2Mn]^+$ and $[Tp^*{}_2Mn]^+$ complexes with $S = 1$, their actual spin ground state. Here, the D values for the crystallographic and DFT-optimized coordinates differ by only ∼0.5 cm^{-1}, which is insignificant. In contrast, for the $S = 2$ states, the computed D values for $[Tp_2Mn]^+$ and $[Tp^*{}_2Mn]^+$ are dramatically different between the X-ray and geometry-optimized models, and no value resembles that seen for typical six-coordinate Mn(III) complexes with $S = 2$ ground states.[73,94] This latter observation could be a consequence of the fact that the D values are computed here for $S = 2$ Mn(III) centers using the geometries of the corresponding $S = 1$ forms. In any case, the large variation in D between the crystallographic and geometry-optimized models is almost completely due to the spin−orbit coupling contribution (D^{SOC}); specifically, contributions to D^{SOC} from spin-flip transitions change significantly in sign and magnitude. The situation for $[\{PhB(MeIm)_3\}_2Mn]^+$ is less clear. For this complex, the two geometries give for the $S = 1$ state D values differing by ∼3 cm^{-1}, which is significant and arises almost completely from the contribution of spin-flip transitions to D^{SOC}. For both methods, the calculated zfs is disconcertingly small (∼10 cm^{-1}), since, if true, then HFEPR would easily be observed (and the magnetic data correspondingly fitted). For the $S = 2$ state, the two methods applied to $[\{PhB(MeIm)_3\}_2Mn]^+$ give essentially the same results, with a small magnitude, negative D (Table 5), a result much more realistic than those for $[Tp_2Mn]^+$ and $[Tp^*{}_2Mn]^+$. Qualitatively, the calculated zfs results in the $[Tp_2Mn]^+$ and $[Tp^*{}_2Mn]^+$ complexes for $S = 1$ versus $S = 2$, that is, consistency between methods in the triplet state, but not in the quintet, validate the observed $S = 1$ spin ground state, whereas for the tris(carbene)borate complex, no such generalization can be made.

The calculations for $[Tp_2Mn]^+$, $[Tp^*{}_2Mn]^+$, and $[\{PhB(MeIm)_3\}_2Mn]^+$ give D^{SSC} in the range of 1.0−1.8 cm^{-1}, thus roughly 5−10% of the total D values, which is significant, but not as critically important an effect as in, for example, Mn(II).[82−85] Thus, their omission in the LFT analysis described above is not serious.

Clearly, QCT at the level of DFT and UHF gives only a shallow insight into these complexes, especially the magnetic parameters. A complete QCT analysis of these Mn(III) complexes would require an ab initio treatment, using complete active space self-consistent field (CASSCF)-based methods and second-order N-electron valence state perturbation theory (NEVPT2), as done by Neese and co-workers for other HS complexes, such as of Fe(II),[95] V(III),[67] Ni(II),[96] and especially on an extensive series of Mn(III), albeit with "traditional", $S = 2$ ground states.[92] The results of such ab initio methods can then be used to calculate LFT (AOM) parameters, as was beautifully shown by Atanasov et al. for trigonal HS Fe(II) complexes.[95] Such an effort would be particularly useful for the tris(carbene)borate complex, which we have demonstrated to show some evidence of possessing an orbitally degenerate ground state. Such a ground state is totally unsuitable for DFT, as pointed out by Neese and co-workers.[50,81,87,97,98] Calculations of that sophistication are beyond the scope of the current study, but we plan them in future work and also hope to inspire others in this effort.

dx.doi.org/10.1021/ic301630d | Inorg. Chem. 2013, 52, 144−159

CONCLUSIONS

The trigonally distorted octahedral Mn(III) complexes with bis(scorpionate) ligands, both pyrazolyl (unsubtituted, Tp^-, and 3,5-dimethyl substituted, Tp^{*-}) and imidazolyl (carbene) donors ($PhB(MeIm)_3^-$, complex $[\{PhB(MeIm)_3\}_2Mn]X$ (X = CF_3SO_3, Cl) have been investigated by a variety of techniques, including magnetometry, electronic absorption spectroscopy, and, for the first time, HFEPR. We have also applied a complementary frequency-domain technique, FD-FT THz-EPR, with the energy source being coherent synchrotron radiation, to $[Tp_2Mn]SbF_6$ (**1**). Gratifyingly, the results for **1** using magnetometry, HFEPR, and FD-FT THz-EPR were in excellent agreement. The synthesis of a previously unreported complex, $[\{PhB(MeIm)_3\}_2Mn]Cl$ (**3b**), is described. These complexes, in contrast to many octahedral complexes of Mn(III), exhibit spin triplet ground states, rather than the spin quintet of HS Mn(III), which is observed in classical six-coordinate Mn(III) complexes, such as $Mn(acac)_3$. The spin triplet ground state in the tris(pyrazolyl)borate complexes $[Tp_2Mn]SbF_6$ (**1**) and $[Tp^*_2Mn]SbF_6$ (**2**) is characterized by a large, positive zfs, which has been rationalized by both LFT and DFT analysis in a manner consistent with results for other such complexes. The tris(carbene)borate (tris(imidazolyl)borate) complexes, $[\{PhB(MeIm)_3\}_2Mn]X$ (X = CF_3SO_3, Cl, **3a** and **3b**, respectively), also have a spin triplet ground state, supported by theory, but in contrast to the tris(pyrazolyl)borate complexes, it likely has large zfs, which is postulated to be the result of strong σ-donation and little, if any, π interaction from this unusual ligand. Now that the electronic structure of these systems has been characterized experimentally, we believe that these are good candidates for investigation by the latest ab initio computational methods, which have hitherto been applied primarily to first row transition-metal ions with "normal" spin ground states (e.g., quintet Mn(III)[92] and sextet Mn(II)[85,99]).

ASSOCIATED CONTENT

Supporting Information

Tables containing metrical parameters, UHF results, Ligfield program output files, and ORCA program DFT input/output file and figures showing the molecular structure of the cation of **1**, the solution electronic absorption spectra of **1**, **2**, and **3a**, and the MOs calculated by DFT for the cation of **1**. This material is available free of charge via the Internet at http://pubs.acs.org.

AUTHOR INFORMATION

Corresponding Author

*E-mail: jesmith@nmsu.edu (J.M.S.); jtelser@roosevelt.edu (J.T.).

Notes

The authors declare no competing financial interest.

ACKNOWLEDGMENTS

This work has been supported by the ACS-PRF (J.M.S. and T.A.J.), the Department of Energy, Office of Basic Energy Sciences (DE-FG02-08ER15996) (J.M.S.), the Camille and Henry Dreyfus Foundation (J.M.S.), and by the NHMFL, which is funded by NSF (Cooperative Agreement DMR 0654118), the State of Florida, and DOE. Additional NHMFL funding was obtained through User Collaboration Grant 5062 (J.K. and J.T.). The 25-T magnet at NHMFL was funded by the W. M. Keck Foundation, and the UV–vis-NIR spectrophotometer at Roosevelt University was funded by the Goldenberg Foundation. We are grateful to Prof. Frank A. Schultz (IUPUI) for generously providing samples of **1** and **2**. We thank Ms. Charlotte Stern (Integrated Molecular Structure Education and Research Center (IMSERC), Northwestern University, which is supported by NSF) for determination of the unit cell parameters of crystals of **1** and **2** synthesized at Roosevelt University. S.A.Z. acknowledges support of the DFG and EuroMagNet II (EU Contract 228043). FD-FT THz-EPR measurements were supported by the German Ministry of Education and Research (BMBF) within the network project EPR-Solar (03SF0328). We thank Prof. Robert Bittl (Freie Universität Berlin) for providing access to the FTIR spectrometer and the magnet used for these measurements. J.M.S. thanks Prof. Jeffrey R. Long (UC-Berkeley) for generous hospitality during a sabbatical stay.

DEDICATION

This paper is dedicated to the memory of Philip L. W. Tregenna-Piggott (1968–2010).

REFERENCES

(1) Ligand abbreviations used: Tp^- = hydrotris(pyrazolyl)borate anion, Tp^{*-} = hydrotris(3,5-dimethylpyrazolyl)borate; $PhB(MeIm)_3^-$ = phenyltris(3-methylimidazol-2-yl)borate.

(2) Trofimenko, S. *Scorpionates: The Coordination Chemistry of Polypyrazolylborate Ligands*; Imperial College Press: London, U.K., 1999; p 292.

(3) Trofimenko, S. *Polyhedron* **2004**, *23*, 197–203.

(4) Pettinari, C. *Scorpionates II: Chelating Borate Ligands*; World Scientific: London, U.K., 2008; p 548.

(5) Spicer, M. D.; Reglinski, J. *Eur. J. Inorg. Chem.* **2009**, 1553–1574.

(6) Smith, J. M. *Comments Inorg. Chem.* **2008**, *29*, 189–233.

(7) Riordan, C. G. *Coord. Chem. Rev.* **2010**, *254*, 1815–1825.

(8) Nieto, I.; Cervantes-Lee, F.; Smith, J. M. *Chem. Commun.* **2005**, 3811–3813.

(9) Cowley, R. E.; Bontchev, R. P.; Duesler, E. N.; Smith, J. M. *Inorg. Chem.* **2006**, *45*, 9771–9779.

(10) Nieto, I.; Bontchev, R. P.; Ozarowski, A.; Smirnov, D.; Krzystek, J.; Telser, J.; Smith, J. M. *Inorg. Chim. Acta* **2009**, *362*, 4449–4460.

(11) Myers, W. K.; Duesler, E. N.; Tierney, D. L. *Inorg. Chem.* **2008**, *47*, 6701–6710.

(12) Myers, W. K.; Scholes, C. P.; Tierney, D. L. *J. Am. Chem. Soc.* **2009**, *131*, 10421–10429.

(13) Hossain, F.; Rigsby, M. A.; Duncan, C. T.; Milligan, P. L.; Lord, R. L.; Baik, M.-H.; Schultz, F. A. *Inorg. Chem.* **2007**, *46*, 2596–2603.

(14) Krivokapic, I.; Noble, C.; Klitgaard, S.; Tregenna-Piggott, P. L. W.; Weihe, H.; Barra, A.-L. *Angew. Chem., Int. Ed.* **2005**, *44*, 3613–3616.

(15) Forshaw, A. P.; Bontchev, R. P.; Smith, J. M. *Inorg. Chem.* **2007**, *46*, 3792–3794.

(16) Xing, Y. H.; Aoki, K.; Bai, F. Y. *Synth. React. Inorg. Met.-Org. Chem.* **2004**, *34*, 1149–1163.

(17) Found here for $[Tp_2Mn]SbF_6$ (**1**; distances in Å, angles in deg): a = 7.492(7), b = 8.802(9), c = 9.918(9); α = 99.05(2), β = 91.75(2), γ = 108.46(2), volume = 610.346 Å^3; previously reported[13] (CSD code: PIBMUJ): a = 7.5518(2), b = 8.8710(2), c = 9.9838(3), α = 99.097(1), β = 91.782(1), γ = 108.516(1), volume = 623.87 Å^3.

(18) Found here for $[Tp^*_2Mn]SbF_6$ (**2**, distances in Å, angles in deg): a = 10.518(8), b = 14.334(10), c = 12.554(9), α = 90.000, β = 94.329(16), γ = 90.000, volume = 1887.383 Å^3; previously reported[13] (CSD code: PIBNAQ): a = 10.4142(4), b = 14.1854(6), c = 12.4063(5), α = 90.000, β = 94.2700(10), γ = 90.000, volume = 1827.69 Å^3.

(19) *APEX*, 2009.1; Bruker AXS, Inc.: Madison, WI, 2009.

(20) Sheldrick, G. M. *SADABS*, 2.03; Bruker AXS, Inc.: Madison, WI, 2000.

(21) Sheldrick, G. M. *SHELXTL*, 6.12; Bruker AXS, Inc.: Madison, WI, 2001.
(22) van der Sluis, P.; Spek, A. L. *Acta Crystallogr.* **1990**, *A46*, 194−201.
(23) Though these constants are well-established in a variety of references, Bain and Berry[24] provide an exceptional collection of almost all useful values for the necessary calculations.
(24) Bain, G. A.; Berry, J. F. *J. Chem. Educ.* **2008**, *85*, 532−536.
(25) Hassan, A. K.; Pardi, L. A.; Krzystek, J.; Sienkiewicz, A.; Goy, P.; Rohrer, M.; Brunel, L.-C. *J. Magn. Reson.* **2000**, *142*, 300−312.
(26) Zvyagin, S. A.; Krzystek, J.; van Loosdrecht, P. H. M.; Dhalenne, G.; Revcolevschi, A. *Phys. Rev. B* **2003**, *67*, 212403.
(27) Krzystek, J.; Zvyagin, S. A.; Ozarowski, A.; Trofimenko, S.; Telser, J. *J. Magn. Reson.* **2006**, *178*, 174−183.
(28) Abragam, A.; Bleaney, B. *Electron Paramagnetic Resonance of Transition Ions*; Dover Publications, Inc.: Mineola, NY, 1986.
(29) Abo-Bakr, M.; Feikes, J.; Holldack, K.; Kuske, P.; Peatman, W. B.; Schade, U.; Wüstefeld, G.; Hübers, H. W. *Phys. Rev. Lett.* **2003**, *90*, 094801.
(30) Schnegg, A.; Behrends, J.; Lips, K.; Bittl, R.; Holldack, K. *Phys. Chem. Chem. Phys.* **2009**, *11*, 6820−6825.
(31) Ballhausen, C. J. *Introduction to Ligand Field Theory*; McGraw-Hill: New York, 1962; pp 99−103.
(32) Schäffer, C. E. *Struct. Bonding (Berlin, Ger.)* **1968**, *5*, 68−95.
(33) Figgis, B. N.; Hitchman, M. A. *Ligand Field Theory and its Applications*; Wiley-VCH: New York, 2000.
(34) Bendix, J.; Brorson, M.; Schäffer, C. E. *Inorg. Chem.* **1993**, *32*, 2838−2849.
(35) Mabbs, F. E.; Collison, D. *Electron Paramagnetic Resonance of d Transition Metal Compounds*; Elsevier: Amsterdam, 1992.
(36) Brorson, M.; Schäffer, C. E. *Inorg. Chem.* **1988**, *27*, 2522−2530.
(37) Brorson and Schäffer have their own parametrization of interelectronic repulsion, but their values can be easily converted to Racah parameters. Theirs are the values listed by Figgis and Hitchman.[33]
(38) Fujihara, T.; Schönherr, T.; Kaizaki, S. *Inorg. Chim. Acta* **1996**, *249*, 135−141.
(39) Neese, F. *ORCA: An ab initio, density functional and semiempirical program package, 2.9*; Universität Bonn: Bonn, Germany, 2010.
(40) Becke, A. D. *J. Chem. Phys.* **1986**, *84*, 4524−4529.
(41) Perdew, J. P. *Phys. Rev. B* **1986**, *33*, 8822−8824.
(42) Perdew, J. P. *Phys. Rev. B* **1986**, *34*, 7406.
(43) Becke, A. D. *Phys. Rev. A* **1988**, *38*, 3098−3100.
(44) Lee, C.; Yang, W.; Parr, R. G. *Phys. Rev. B* **1988**, *37*, 785−789.
(45) Weigend, F.; Ahlrichs, R. *Phys. Chem. Chem. Phys.* **2005**, *7*, 3297−3305.
(46) Schäfer, A.; Horn, H.; Ahlrichs, R. *J. Chem. Phys.* **1992**, *97*, 2571−2577.
(47) Neese, F.; Wennmohs, F.; Hansen, A.; Becker, U. *Chem. Phys.* **2009**, *356*, 98−109.
(48) Eichkorn, K.; Treutler, O.; Öhm, H.; Häser, M.; Ahlrichs, R. *Chem. Phys. Lett.* **1995**, *240*, 283−289.
(49) Eichkorn, K.; Weigend, F.; Treutler, O.; Ahlrichs, R. *Theor. Chem. Acc.* **1997**, *97*, 119−124.
(50) Neese, F. *J. Chem. Phys.* **2007**, *127*, 164112.
(51) Neese, F. *J. Am. Chem. Soc.* **2006**, *128*, 10213−10222.
(52) Laaksonen, L. *J. Mol. Graphics* **1992**, *10*, 33−34.
(53) Bergman, D. L.; Laaksonen, L.; Laaksonen, A. *J. Mol. Graphics Modell.* **1997**, *15*, 301−306.
(54) The reduction potentials ($E^{\circ\prime}$, in V) for the Mn(III)/Mn(II) couple (vs $Fc^{+/0}$) for $[Tp_2Mn]^+$, $[Tp^*_2Mn]^+$, and $[\{PhB(MeIm)_3\}_2Mn]^+$ are, respectively, +0.14,[13] −0.01,[13] and −2.09.[15]
(55) Chan, M. K.; Armstrong, W. H. *Inorg. Chem.* **1989**, *28*, 3777−3779.
(56) In these complexes, there is a substantial (~0.27 Å) increase in bond lengths upon reduction to Mn(II).
(57) DeAlwis, D. C. L.; Schultz, F. A. *Inorg. Chem.* **2003**, *42*, 3616−3622.
(58) These two studies by Schultz and co-workers, respectively, employed different counteranions, $[Tp^*_2Mn]X$, where X = PF_6^- or SbF_6^-, and different solvents, 1,2-dichloroethane[57] versus MeCN.[13]
(59) Jesson, J. P.; Trofimenko, S.; Eaton, D. R. *J. Am. Chem. Soc.* **1967**, *89*, 3148−3158.
(60) Bands nearer to 200 nm are due to intraligand $\pi-\pi^*$ transitions.
(61) Sim, P. G.; Sinn, E. *J. Am. Chem. Soc.* **1981**, *103*, 241−243.
(62) Morgan, G. G.; Murnaghan, K. D.; Müller-Bunz, H.; McKee, V.; Harding, C. J. *Angew. Chem., Int. Ed.* **2006**, *45*, 7192−7195.
(63) Wang, S.; Ferbinteanu, M.; Marinescu, C.; Dobrinescu, A.; Ling, Q.-D.; Huang, W. *Inorg. Chem.* **2010**, *49*, 9839−9851.
(64) Lord, R. L.; Schultz, F. A.; Baik, M.-H. *J. Am. Chem. Soc.* **2009**, *131*, 6189−6197.
(65) Klokishner, S. I.; Roman, M. A.; Reu, O. S. *Inorg. Chem.* **2011**, *50*, 11394−11402.
(66) Krzystek, J.; Park, J.-H.; Meisel, M. W.; Hitchman, M. A.; Stratemeier, H.; Brunel, L.-C.; Telser, J. *Inorg. Chem.* **2002**, *41*, 4478−4487.
(67) Ye, S.; Neese, F.; Ozarowski, A.; Smirnov, D.; Krzystek, J.; Telser, J.; Liao, J.-H.; Hung, C.-H.; Chu, W.-C.; Tsai, Y.-F.; Wang, R.-C.; Chen, K.-Y.; Hsu, H.-F. *Inorg. Chem.* **2010**, *49*, 977−988.
(68) Krzystek, J.; Ozarowski, A.; Telser, J. *Coord. Chem. Rev.* **2006**, *250*, 2308−2324.
(69) Three peaks develop in each branch, and it would be tempting to assign these to g_x, g_y, g_z (or, more generally, g_{max}, g_{mid}, g_{min}). This is reasonable for the outer peaks of each branch, but this assignment for the central peak would require a **g** matrix that is more rhombic than can be allowed by the HFEPR data. We must note that the *g* values were determined from HFEPR fits over a wide field range, whereas the FD-FT THz-EPR spectra are over a narrow field range where zfs dominates over Zeeman effects.
(70) Massa, W.; Babel, D. *Chem. Rev.* **1988**, *88*, 275−296.
(71) Gerritsen, H. J.; Sabisky, E. S. *Phys. Rev.* **1963**, *132*, 1507−1512.
(72) Tregenna-Piggott, P. L. W.; Weihe, H.; Barra, A.-L. *Inorg. Chem.* **2003**, *42*, 8504−8508.
(73) Krzystek, J.; Yeagle, G.; Park, J.-H.; Meisel, M. W.; Britt, R. D.; Brunel, L.-C.; Telser, J. *Inorg. Chem.* **2003**, *42*, 4610−4618.
(74) Alexander, J. J.; Gray, H. B. *J. Am. Chem. Soc.* **1968**, *90*, 4260−4271.
(75) Buschmann, W. E.; Liable-Sands, L.; Rheingold, A. L.; Miller, J. S. *Inorg. Chim. Acta* **1999**, *284*, 175−179.
(76) Krzystek, J.; Swenson, D. C.; Zvyagin, S. A.; Smirnov, D.; Ozarowski, A.; Telser, J. *J. Am. Chem. Soc.* **2010**, *132*, 5241−5253.
(77) For $[Tp_2Cr]^+$, Fujihara et al.[38] used similar values: $\theta = 61°$, $\theta = 58.8°$, and $\psi = 2°$. We have reproduced the results presented in their Table 3, which indicates that our approach is consistent with theirs. Our lack of comparable electronic absorption data for the three Mn(III) scorpionate complexes means that refinements, such as inclusion of nonzero ψ, lead to overparameterization.
(78) Their specific bonding parameters (all in cm^{-1}) for $[Tp_2Cr]^+$ were $\varepsilon_\sigma = 8350$, $\varepsilon_{\pi s} = 1300$. Use of the Δ values based on the solid-state data gives $\varepsilon_\sigma = 8040$, $\varepsilon_{\pi s} = 1260$ and $\varepsilon_\sigma = 7830$, $\varepsilon_{\pi s} = 1220$, respectively, for $[Tp_2Mn]^+$ and $[Tp^*_2Mn]^+$.
(79) These, and subsequent, designations are made assuming idealized D_3 point group symmetry; for D_{3d} symmetry, these would all be "*g*" as well.
(80) McGarvey, B. R.; Telser, J. *Inorg. Chem.* **2012**, *51*, 6000−6010.
(81) Ganyushin, D.; Neese, F. *J. Chem. Phys.* **2006**, *125*, 024103.
(82) Duboc, C.; Phoeung, T.; Zein, S.; Pécaut, J.; Collomb, M.-N.; Neese, F. *Inorg. Chem.* **2007**, *46*, 4905−4916.
(83) Zein, S.; Neese, F. *J. Phys. Chem. A* **2008**, *112*, 7976−7983.
(84) Zein, S.; Duboc, C.; Lubitz, W.; Neese, F. *Inorg. Chem.* **2008**, *47*, 134−142.
(85) Duboc, C.; Collomb, M.-N.; Neese, F. *Appl. Magn. Reson.* **2010**, *37*, 229−245.
(86) For example, in the case of **1**, use of the real θ values (see Table S2, Supporting Information) with the smaller Racah parameters (see Table 3) gave $D = +17.781$ cm^{-1}, with $E = 0.007$ cm^{-1}, a much smaller

rhombicity than from experiment, but this is only the most obvious deviation that could be introduced.
(87) Neese, F. *J. Biol. Inorg. Chem.* **2006**, *11*, 702−711.
(88) Ghosh, A. *J. Biol. Inorg. Chem.* **2006**, *11*, 712−724.
(89) Zerner, M. C.; Martin, C. H. In *Inorganic Electronic Structure and Spectroscopy*; Solomon, E. I., Lever, A. B. P., Eds.; Wiley: New York, 1999; Vol. *I*, p 661.
(90) Neese, F. *Curr. Opin. Chem. Biol.* **2003**, *7*, 125−135.
(91) Neese, F. *J. Chem. Phys.* **2005**, *122*, 034107.
(92) Duboc, C.; Ganyushin, D.; Sivalingam, K.; Collomb, M.-N.; Neese, F. *J. Phys. Chem. A* **2010**, *114*, 10750−10758.
(93) The UHF calculations (see Table S4, Supporting Information) predict *D* values that are too large by ∼30−40%.
(94) Aromí, G.; Telser, J.; Ozarowski, A.; Brunel, L.-C.; Krzystek, J. *Inorg. Chem.* **2005**, *44*, 187−196.
(95) Atanasov, M.; Ganyushin, D.; Pantazis, D. A.; Sivalingam, K.; Neese, F. *Inorg. Chem.* **2011**, *50*, 7460−7477.
(96) Desrochers, P. J.; Sutton, C. A.; Abrams, M. L.; Ye, S.; Neese, F.; Telser, J.; Ozarowski, A.; Krzystek, J. *Inorg. Chem.* **2012**, *51*, 2793−2805.
(97) Neese, F.; Petrenko, T.; Ganyushin, D.; Olbrich, G. *Coord. Chem. Rev.* **2007**, *251*, 288−327.
(98) Neese, F. *Coord. Chem. Rev.* **2009**, *253*, 526−563.
(99) Duboc, C.; Collomb, M.-N.; Pécaut, J.; Deronzier, A.; Neese, F. *Chem.—Eur. J.* **2008**, *14*, 6498−6509.